Applied Energy 253 (2019) 113614

Contents lists available at ScienceDirect

Applied Energy

journal homepage: www.elsevier.com/locate/apenergy

Geographical optimization of variable renewable energy capacity in China using modern portfolio theory

Jing Hu*, Robert Harmsen, Wina Crijns-Graus, Ernst Worrell

Copernicus Institute of Sustainable Development, Utrecht University, Princetonlaan 8a, 3584 CB Utrecht, the Netherlands

HIGHLIGHTS

- Best VRE resources in China were found in Inner-Mongolia and North China.
- Optimal VRE portfolios in China capture geographical smoothing.
- 1.4–5.5% of portfolio capacity can be available 100% of the time.
- Wind and solar complement each other in reducing volatility.
- Portfolios with pre-defined technology shares might be sub-optimal.

ARTICLE INFO

Keywords:
Variable renewable electricity
Efficient frontier
Portfolio
Geographical smoothing
Capacity factor
Geographical potentials

ABSTRACT

The large-scale deployment of wind and solar, which are variable renewable electricity (VRE) technologies, is indispensable to decarbonise China's power sector. However, variability in VRE outputs poses challenges in power system operation in terms of increased demand for backup and reserve capacity. These challenges can be effectively mitigated by "geographical smoothing", because spreading VRE deployment over a large area largely reduces the variability associated with the collective output of VRE. Based on meteorological reanalysis data, this study characterised the return and volatility (i.e. mean and standard deviation of hourly capacity factor) per VRE asset in China at a high-resolution grid cell level. This enabled to identify the efficient frontier of optimal VRE portfolios that capture the geographical smoothing effect for China's future power system, using modern portfolio theory. The portfolio volatility is minimized for each attainable return. We analysed key statistics of optimal portfolios, including technology shares, levelized cost of electricity and capacity factor at-risk values. Our results show complementarity between wind and solar in China, reflected in more optimal return-volatility performance of wind & solar portfolios, as compared to wind-only and solar-only portfolios. In addition, our results show that portfolios with unconstrained technology shares perform much better in return-volatility performance than portfolios with constrained technology shares. This suggests existing scenarios in literature with pre-defined shares of different VRE technologies might be sub-optimal. This study also shows that for optimal wind & solar portfolios a "firm" non-zero minimum portfolio capacity factor (1.4–5.5%) can exist with 100% availability.

1. Introduction

1.1. Background

Deep decarbonization of the power sector is essential for reaching the Paris Agreement target to limit the global mean temperature increase to 1.5–2.0 °C (IPCC, 2014; UNFCCC, 2015). Along with other zero- or low-carbon electricity generation technologies (e.g. hydro, biomass, nuclear, carbon capture and storage), the large-scale deployment of variable renewable electricity (VRE) technologies such as wind and solar photovoltaics (PV) is vital in our bid to decarbonize the power sector [1,2]. The past decade has witnessed fast and robust development in VRE: globally, the total installed capacity of wind and solar PV combined has increased from 102 GW to 941 GW between 2007 and 2017 [3]. Considering the substantial cost reduction resulting from technological learning and economies of scale [4], post-Fukushima safety concerns about nuclear [5] and the lack of commercial track records associated with carbon capture and storage [6], it is

* Corresponding author.
E-mail address: j.hu@uu.nl (J. Hu).

https://doi.org/10.1016/j.apenergy.2019.113614
Received 21 April 2019; Received in revised form 9 July 2019; Accepted 23 July 2019
Available online 06 August 2019

Nomenclature

A	wind turbine sweeping area (m^2)
a	capital recovery factor
Alb	surface albedo
A_{PV}	PV panel area (m^2/kW)
AST	apparent solar time (hour)
BRL	Boland–Ridley–Lauret
C	total installed capacity (GW)
CF	hourly capacity factor
CF_0	hourly capacity factor at sea level
$CF_{100\%}$	CF-at-risk at 100% availability of time
$CF_{90\%}$	CF-at-risk at 90% availability of time
CF_h	hourly capacity factor at elevation
$CF_{h,t}$	hourly capacity factor at elevation for specific time t
$\overline{CF_j}$	average capacity factor for technology j
$CF_{k,t}$	hourly capacity factor of VRE asset k for specific time t
$CF_{p,t}$	portfolio hourly capacity factor for specific time t
C_j	total installed capacity of technology j
cov	covariance matrix
$cov_{k,m}$	covariance between asset k and m
C_p	power coefficient of wind turbine
D	wind turbine rotor diameter (m)
d	displacement height (m)
df	hourly diffuse fraction
DS	day-light saving time (hour)
ET	equation of time (hour)
h	elevation (km)
h_{hub}	wind turbine hub height (m)
H	hour angle (°)
H_0	hourly extraterrestrial horizontal irradiance (W/m^2)
$H_{0,t}$	hourly extraterrestrial horizontal irradiance for specific time t (W/m^2)
$I_{dif,h}$	diffuse component of hourly global horizontal irradiance (W/m^2)
$I_{dif,p}$	diffuse component of hourly total received irradiance on PV panel (W/m^2)
$I_{dir,p}$	direct component of hourly total received irradiance on PV panel (W/m^2)
$I_{dir,h}$	direct component of hourly global horizontal irradiance (W/m^2)
I_h	hourly global horizontal irradiance (W/m^2)
$I_{h,t}$	hourly global horizontal irradiance for specific time t (W/m^2)
I_j	capital costs for technology j (USD_{2015}/kW)
I_p	hourly total received irradiance on PV panel (W/m^2)
IPAC	integrated policy assessment model
$I_{r,p}$	reflection component of hourly total received irradiance on PV panel (W/m^2)
I_{STC}	solar irradiance under standard test conditions (1000 W/m^2)
k_t	hourly clearness index for specific time t
K_t	daily clearness index for specific time t
L	local latitude (°)
LCOE	levelized cost of electricity (USD_{2015}/MWh)
$LCOE_{j,i}$	LCOE for technology j in grid cell i (USD_{2015}/MWh)
$LCOE_k$	LCOE for VRE asset k (USD_{2015}/MWh)
$LCOE_p$	portfolio LCOE (USD_{2015}/MWh)
LL	local longitude (°)
LST	local standard time (hour)
m	eastward component of wind speed (m/s)
$maxCF_{100\%}$	portfolio with maximum $CF_{100\%}$
$maxCF_{90\%}$	portfolio with maximum $CF_{90\%}$
maxret	maximum return portfolio
minCV	portfolio with minimum coefficient of variation
minvol	minimum volatility portfolio
MPT	modern portfolio theory
n	northward component of wind speed (m/s)
N	day number of the year
O&M	annual fixed operating and maintenance costs (USD_{2015}/kW)
$O\&M_j$	annual fixed O&M costs for technology j (USD_{2015}/kW)
P_j	total potentials for technology j (MW)
$P_{j,i}$	potentials for technology j in grid cell i (MW)
P_k	potentials for VRE asset k (MW)
PR	PV performance ratio
P_{rated}	wind turbine rated power output (MW)
PV	photovoltaics
r	discount rate
SF_i	capital costs scaling factor for grid cell i
SL	standard longitude (°)
S_{rPV}	unit spacing area for rooftop PV (km^2/MW)
$t_{sunrise}$	sunrise time (hour)
t_{sunset}	sunset time (hour)
v	wind speed (m/s)
v_0	wind speed at sea level (m/s)
v_h	wind speed at elevation (m/s)
v_{in}	wind turbine cut-in speed (m/s)
v_{off}	wind turbine cut-off speed (m/s)
v^0_{rated}	wind turbine rated wind speed at sea level (m/s)
v^h_{rated}	wind turbine rated wind speed at elevation (m/s)
VRE	variable renewable electricity
v_{ref}	wind speed at reference height (m/s)
z	height (m)
z_0	surface roughness length (m)
Z_p	panel azimuth angle (°)
z_{ref}	reference height (m)
Z_s	solar azimuth angle (°)
$Z_{s,ref}$	reference solar azimuth angle (°)
α	solar altitude angle (°)
α_{ref}	reference solar altitude angle (°)
β	panel tilt angle (°)
ϵ	wind turbine power coefficient correction parameter
δ	declination angle (°)
θ	incidence angle (°)
μ	mean of hourly capacity factor
$\mu_{j,i}$	mean capacity factor for technology j in grid cell i
μ_k	mean capacity factor for VRE asset k
μ_p	portfolio return
$\boldsymbol{\mu}^T$	transpose vector of mean capacity factor
ρ	air density (kg/m^3)
ρ_0	reference air density at sea level (1.225 kg/m^3)
ρ_h	air density at elevation (kg/m^3)
σ	standard deviation of hourly capacity factor
σ_p	portfolio volatility
φ	persistence index
$\boldsymbol{\omega}$	vector of contributing weight
ω_j	portfolio share of technology j
ω_k	contributing weight of VRE asset k in portfolio
$\boldsymbol{\omega}^T$	transpose vector of contributing weight

reasonable to foresee that VRE will play a dominant role in the power system of the future.

Wind and solar PV are considered VRE technologies as their production depends on stochastic fluxes of meteorological resources. Integrating VRE into the power system poses challenges in grid operation and results in "integration costs" [7]. Both the variability and

uncertainty of VRE outputs necessitates additional backup capacity, reserve capacity and storage to ensure generation adequacy [8], to follow output ramps [9]and to balance forecast errors [10].

An effective way to mitigate these impacts and reduce integration costs is to disperse the deployment of VRE over a large area with diverse weather patterns [11]. Decreased correlation in weather patterns across greater distances creates the ***geographical smoothing effect*** that largely reduces the variability and uncertainty associated with the output of individual VRE generators [12–15]. This effect can also be strengthened by complementarity between various VRE technology types [12]. Consequently, with geographical smoothing, VRE collectively shows higher firm capacity,[1] a smaller spread of output ramps and lower forecast errors [16,17].

The geographical smoothing effect can be captured by modern portfolio theory (MPT). MPT is a financial theory which helps to guide investment decision-making subject to the trade-off between (expected) return and risk (which is usually represented by the volatility of return) in the market [18]. It is used to obtain the efficient frontier of portfolios of individual financial assets. Because of perfect diversification, any portfolio at the efficient frontier is optimal in the sense that at a given return, risk is minimized, while at a given risk, return is maximized. Fig. 1 illustrates the efficient frontier of 4 assets (bills, bonds, gold and stocks), where each point on the frontier represents an optimal portfolio.

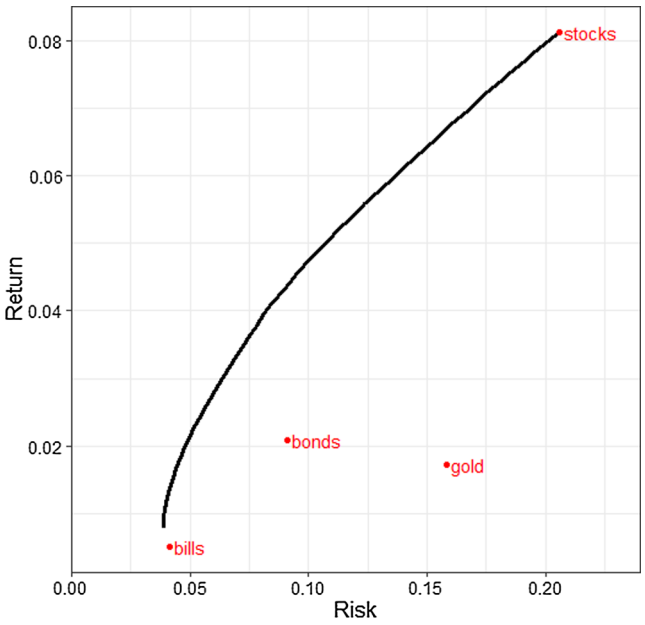

Fig. 1. Illustration of efficient frontier of 4 assets.
Source: Authors' elaboration.

1.2. Literature review

Various authors have adopted MPT to identify the geographically optimal portfolios that spread the VRE capacity of one or more technology types across different locations, to capture the geographical smoothing effect. In this context, a certain type of VRE technology at a specific location becomes an individual **VRE asset**. Return is then usually represented as the (physical) power output of VRE whereas risk can either be output volatility (e.g. [19–23]), or output ramp rate volatility (e.g. [4,24–26]).

When risk is treated as output volatility, i.e. the standard deviation of output across time, optimal portfolios are the minimum volatility portfolio for each possible output level. This is particularly relevant for generation adequacy, which aims to increase VRE's firm capacity and reduce backup capacity. For instance, Shahriari and Blumsack [23] determine the capacity value (defined as the output available for a prespecified percentage of time) for optimal wind and solar portfolios, based on the output duration curve. Degeilh and Singh [21] also calculate the loss of load probability associated with optimal wind portfolios during peak load time. Both papers demonstrate that MPT helps to increase the firm capacity of VRE. When risk is treated as output ramp rate volatility, i.e. the standard deviation of output ramp rate, it enables us to identify optimal portfolios that can reduce the spread and extreme values of VRE ramp events [27]. Hence, MPT is useful for saving reserve capacity from the perspective of system reliability. Alternatively, Speth [28] and Lima et al. [29] also use MPT to increase the predictability of VRE. In their studies, return and risk are respectively framed as average forecast errors and the standard deviation of forecast errors across time.

The representation of VRE assets in MPT literature is either based on pre-selected sites (of existing and planned power plants) or on a uniform grid cell. Many studies adopt the former representation, and they often rely on site-specific output measurement data or pre-developed simulation data from literature. By contrast, Thomaidis et al. [30]; Tejeda et al. [22]; Koivisto et al. [19] use meteorological data to simulate VRE outputs at uniform grid cell level. This representation is more advantageous, as it enables the portfolio to include VRE assets in all sites, especially in sites without measurement data.

Due to data limitation and modelling complexity, most studies do not explicitly consider transmission constraints through a copperplate assumption. Among few analyses factoring into transmission constraints, the treatment of transmission constraints varies. Roques et al. [26] formulate cross-border transmission capacity as an additional constraint condition for net imports in the MPT optimization, while Rombauts et al. [31] add transmission capacity in the optimization objective function by introducing variables of post-transmission power flows. Alternatively, Novacheck and Johnson [27] use portfolios obtained from MPT optimization as inputs in a power system model to investigate the impact of transmission constraints. They conclude that even if transmission constraints are not represented in the MPT optimization, MPT-based portfolios alleviate transmission congestion due to diversification.

A thorough overview of recent MPT literature is presented in Table 1. It assesses different studies according to their return-risk framework, temporal and spatial resolution, geographical scope, inclusion of technology, representation of VRE assets, and treatment of transmission constraints.

1.3. Knowledge gap and research objective

While MPT-based studies have been performed for a limited number of regions in the world (e.g. England [20]; Southern Iberian Peninsula [30]; Germany [28]; Spain [32]; Northern Europe [19]; the combined area of Austria, Denmark, France, Germany and Spain [26]; European Union [22]; Eastern Interconnection of United States [23]), to the authors' best knowledge no such study is yet available for China. China has the largest cumulative installed VRE capacity [3]. With support from the Chinese government, the momentum of rapid VRE development is likely to continue [33]. However, even today China has already faced severe curtailment problem of VRE generation due to insufficient capability to manage VRE volatility [34]. Therefore, fully exploiting the geographical smoothing effect is essential and pertinent to plan optimal VRE development in China's low-carbon transition. To fill the knowledge gap of the absence of MPT-based study for China, this research aims to explore optimal VRE portfolios that capture the geographical smoothing effect in China's long-term future power system. It also aims

[1] Firm capacity can be defined as the fraction of VRE's nameplate capacity that can replace conventional power plants without changing the system reliability.

Table 1
Overview of recent MPT-based studies.
Source: Compiled based on Drake and Hubacek [20], Roques et al. [26], Rombauts et al. [31], Degeilh and Singh [21], Speth [28], Thomaidis et al. [30], Santos-Alamillos et al. [32], Novacheck and Johnson [27], Tejeda et al. [22], Lima et al. [29], Shahriari and Blumsack [23], and Koivisto et al. [19].

Study	Return-risk framework		Resolution		Geographical scope	Inclusion of technology	Representation of VRE assets	Treatment of transmission constraints
	Return	Risk	Temporal	Spatial				
Drake and Hubacek [20]	Physical output of VRE	Standard deviation of output	Hourly	Site level	UK	Offshore wind	Pre-selected sites	Copperplate
Roques et al. [26]	Physical output of VRE	Standard deviation of output and output ramp	Hourly	Aggregated to country level	Combined area of Austria, Denmark, France, Germany and Spain	Onshore and offshore wind	Pre-selected sites	Formulated as constraints for net imports
Rombauts et al. [31]	Physical output of VRE	Standard deviation of output ramp	Hourly	Site level	NA (three fictitious countries)	Onshore wind	Pre-selected sites (sampled from the Netherlands)	Considered in optimization objective by introducing post-transmission power flows
Degeilh and Singh [21]	Physical output of VRE	Standard deviation of output and output ramp	Hourly	Site level	Two areas considered separately: 7 sites in West Texas; 7 sites in Western United States	Onshore wind	Pre-selected sites	Copperplate
Speth [28]	Physical output of VRE; average forecast errors	Standard deviation of output and output ramp; standard deviation of forecast errors	Hourly	Site level	Germany	Wind and PV (without detailed technology specifications)	Pre-selected sites	Copperplate
Thomaidis et al. [30]	Physical output of VRE	Standard deviation of output	Hourly	9 km * 9 km	Southern Iberian Peninsula	Onshore wind and concentration solar power	Uniform grid cell	Copperplate
Santos-Alamillos et al. [32]	Physical output of VRE	Standard deviation of output	Hourly	Site level but calibrated to 5 km * 5 km grid cell	Spain	Onshore wind	Pre-selected sites	Copperplate
Novacheck and Johnson [27]	Physical output of VRE	Standard deviation of output ramp	Hourly	Site level	Midwestern United States	Onshore wind	Pre-selected sites	Modelling of power system after optimization
Tejeda et al. [22]	Physical output of VRE	Standard deviation of output	6-hourly	0.25° * 0.25°	European Union	Onshore and offshore wind	Uniform grid cell	Copperplate
Lima et al. [29]	Average forecast errors	Standard deviation of forecast errors	Hourly	Site level	Northeastern Brazil	Wind and PV (without detailed technology specifications)	Pre-selected sites	Copperplate
Shahriari and Blumsack [23]	Physical output of VRE	Standard deviation of output	10-min, hourly, daily, weekly and monthly	Site level	Eastern Interconnection of United States	Wind and PV (without detailed technology specifications)	Pre-selected sites	Copperplate
Koivisto et al. [19]	Physical output of VRE	Standard deviation of output	Hourly	Site level but calibrated to 10 km * 10 km grid cell	Northern Europe	Onshore and offshore wind, PV (without detailed technology specifications)	Pre-selected sites for wind and uniform grid cell for PV	Copperplate

to generate in-depth insights of optimal portfolios' properties through analysis of key portfolio statistics (e.g. levelized cost of electricity, value-at-risk of capacity factor), which can be used to support the decision-making in power system investment and operation. The year 2050 is indicatively selected as the target year, since it is often used to set long-term energy/climate targets in many scenario-based studies (e.g. [35,36]). In this paper geographical smoothing is defined as the minimum output volatility for each possible output level. The novelty of this study is that we explicitly consider four types of VRE (onshore wind, offshore wind, utility-PV and rooftop PV) and use high-resolution (0.5° * 0.667°) meteorological reanalysis data[2] that covers all locations in China to simulate VRE outputs at a uniform grid cell level. This adds to previous studies that (1) tend to focus on only one VRE technology type [20,22,26–28], (2) build up portfolios based on pre-selected VRE sites [20,23,26,27], and (3) use low-resolution data to aggregate VRE outputs [22,26]. The entire China region[3] (including neighboring areas and exclusive economic zone) is divided into 7938 grid cells with a spatial resolution of 0.5° * 0.667° to match the reanalysis data. Constructing optimal portfolios comprising multiple VRE technology types based on high-resolution meteorological reanalysis data has never been done by previous MPT-based studies for a region at such a large geographical scale and across so many climate zones. Therefore, this study expands the application of MPT. It also enables a comprehensive understanding of geographical smoothing by encompassing all locations suitable to develop VRE and by accounting for the complementarity between different VRE technologies, which adds value to scientific literature. The contribution of this paper is threefold. Firstly, it informs policy-makers and academic peers about the performance and potentials of each VRE technology type in China at a high-resolution grid cell level. Secondly, optimal portfolios determined in this study can help policy-makers to plan VRE development and grid expansion in a more system-optimized manner and bring about multiple economic benefits. Lastly, the detailed methodology presented in this paper is reproducible, and can be easily applied to other regions with high VRE potentials, such as India and Africa.

In Section 2 we describe the method used for data processing and post-processing. The results are presented in Section 3. In Section 4 we discuss the limitations and uncertainties of this study, while conclusions are drawn in Section 5.

2. Methods

In this chapter we present the methods applied to carry out the main tasks, five related to the data processing phase (Sections 2.1–2.5) and four related to the post-processing phase (Sections 2.6–2.9). A brief overview of the research design for this paper is presented in Fig. 2. All tasks were performed using RStudio and ArcGIS.

Section 2.1 explains the method for estimating geographical potentials in terms of the maximum capacity (in MW) that can be installed, accounting for different geographical constraints and social acceptance. Section 2.2 describes how to characterize the time series of hourly power output per unit rated power for each VRE asset, referred to as the hourly capacity factor (CF). In Section 2.3 we lay out the method used to determine the average CF weighted by geographical potentials per grid cell in China, per technology. This task combines the results of the previous two tasks. Section 2.4 provides the method used to calculate the levelized cost of electricity (LCOE) per VRE asset, built upon the mean of hourly CF introduced in Section 2.2. Section 2.5 describes applying MPT optimization to determine the efficient frontier of optimal portfolios for various 2050 scenarios.

The four post-processing tasks were carried out to analyse key statistics and performance indicators for selected portfolios positioned on the efficient frontier. This enables comparison and explanation. In Section 2.6 we present the method used to characterize the contributing weights per VRE asset for these portfolios. Sections 2.7 and 2.8 provide the methods used to calculate the portfolio share per VRE technology and the portfolio LCOE. Finally, in Section 2.9, we describe the procedure for how to generate the portfolio CF duration curve and how to determine its Value-at-Risk.

2.1. Data processing task 1: Estimate geographical potentials

The approach we followed to determine the geographical potentials for each VRE asset (defined as a certain VRE technology in a certain grid cell) and the total potentials per VRE technology are described respectively in Sections 2.1.1 and 2.1.2.

2.1.1. Geographical potentials per VRE asset

Estimating the geographical potentials for each VRE asset was based on a three-step procedure (see Fig. 3).

Firstly, based on the territory area of China (which is divided into 7938 grid cells with resolution of 0.5° * 0.667°), we calculated the available area (in km^2) per grid cell after considering multiple geographical constraints (see Table 2). Following Herran et al. [38], we introduced an additional social acceptance constraint specifically for onshore wind and utility-PV. It is defined as a threshold distance from the dense urban area (urban areas > 50%) to restrict visibility impacts that can result in social unacceptance, which we set conservatively at 10 km. Secondly, by using suitability factors for different land cover categories, we further narrowed down the area suitable for deployment of VRE technologies per grid cell (being the multiplication product of the available area and suitability factors). The land cover suitability factors are shown in Table 3. Lastly, based on the unit spacing area per VRE technology, we estimated the maximum capacity that can be installed in each grid cell as geographical potentials. Depending on the turbine rotor diameter (D), the unit spacing area for both onshore and offshore wind can be *narrow* (5.25D * 5.25D), *intermediate* (7D * 7D) and *wide* (10.5D * 10.5D) [39]. We opted to use the intermediate spacing, as it has a relatively low spacing density without incurring large wake losses [25]. The installed turbines were based on three onshore modules (Vestas-112, −117 and −126) with rated capacity of 3.3 MW and one offshore module (Vestas-164) with rated capacity of 8 MW (see Table 4 for details).

Both installed utility-PV and rooftop PV were based on the Sanyo HIP-225HDE1 module with a rated capacity of 0.225kW_p for a total area of 1.39 m^2. As rule-of-thumb, the unit spacing area for utility-PV was set at 1 ha/MW (or 0.01 km^2/MW) [59]. For rooftop PV, based on flat roof assumption[4] we calculated the required unit array spacing that avoids self-shading. Following Copper et al. [60], the hour with the third lowest solar altitude angle on the winter solstice, being the worst-case scenario, was established as the reference condition to calculate the unit spacing area (S_{rPV}) for each grid cell. The calculation was performed with formula (1).

$$S_{rPV} = A_{PV} * (\cos(\beta) + \frac{\sin(\beta)}{\tan(\alpha_{ref})}\cos(Z_{s,ref} - Z_p)) \quad (1)$$

where A_{PV} is the PV panel area; β and $Z_p$are panel tilt angle and azimuth angle; α_{ref} and $Z_{s,ref}$ are solar altitude angle and azimuth angle under the reference condition.

[2] Reanalysis data is weather data simulated by an atmospheric circulation model, which is used to assimilate historical weather observations for hindcasting purpose [37].

[3] The Taiwan area is excluded in this study due to the absence of interconnection with mainland China.

[4] Because of the dominance of flat roof residential buildings in China, especially in cities.

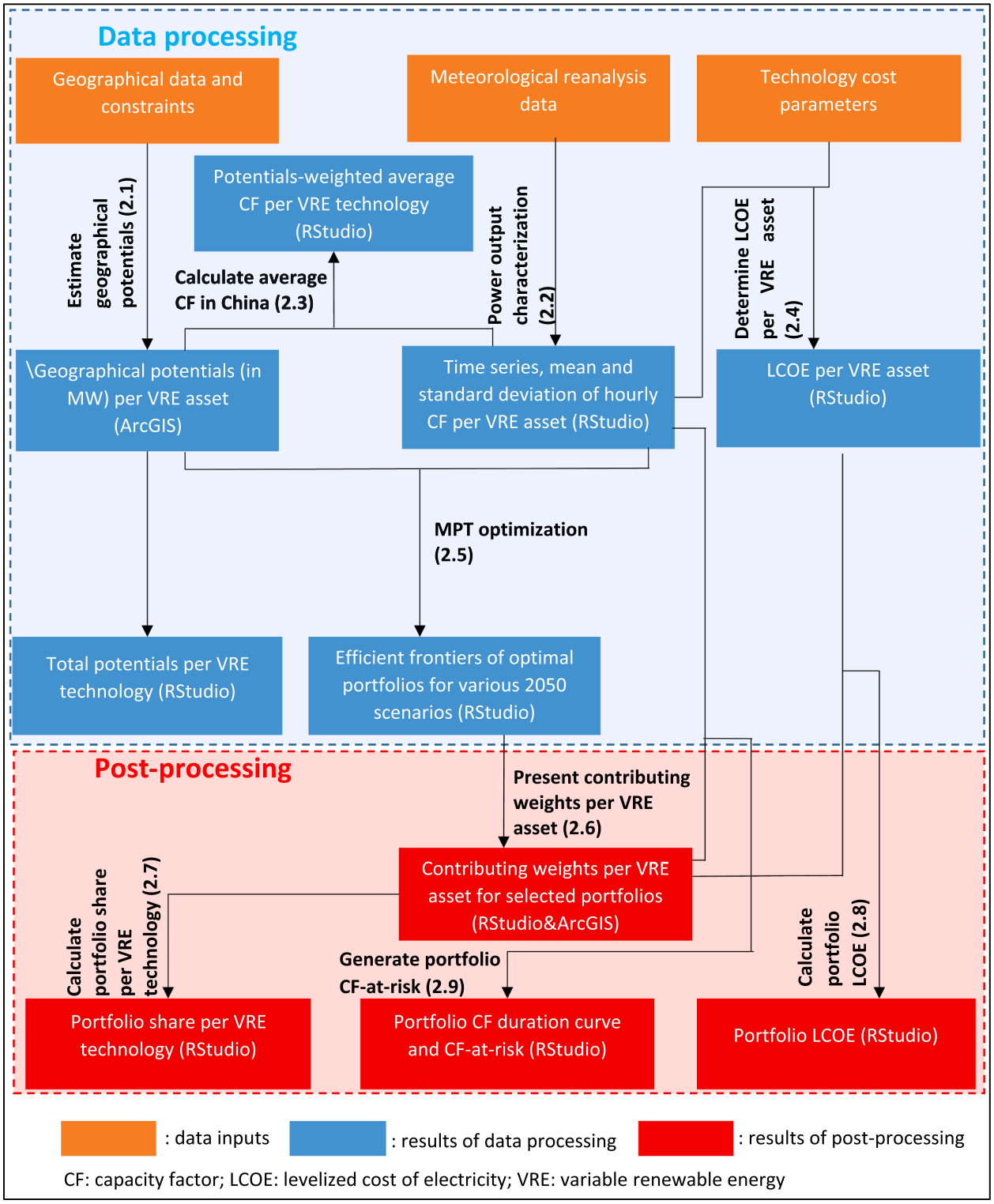

Fig. 2. Overview of research design. Source: Authors' elaboration.

2.1.2. Total potentials per VRE technology

We determined the total potentials per VRE technology through summing the maximum capacity that can be installed in each grid cell:

$$P_j = \sum_i^n P_{j,i}, j = onshore\ \ wind,\ \ \ offshore\ \ wind,\ \ \ utility\_PV,\ \ rooftop\ \ PV \quad (2)$$

where P_j is the total potentials for technology j and $P_{j,i}$ is the geographical potentials for technology j in grid cell i.

Three cases for onshore wind were explicitly considered to reflect the impact of including/excluding the social acceptance constraint (10 km distance from urban area) and the use of different sets of suitability factors, i.e. (1) High potentials (excluding social acceptance constraint + high suitability factors); (2) Medium potentials (including social acceptance constraint + high suitability factors); (3) Low potentials (including social acceptance constraint + low suitability

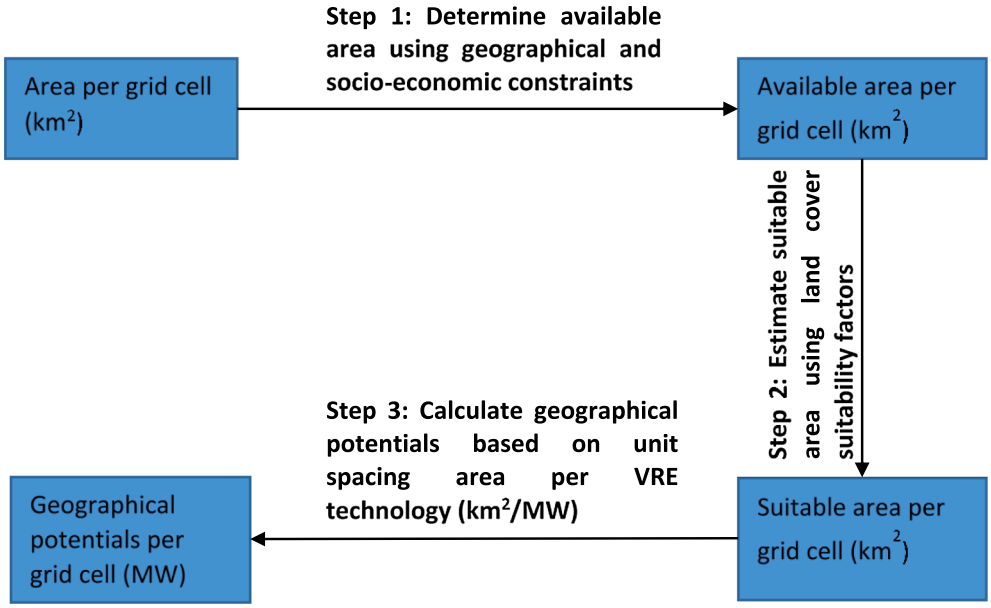

Fig. 3. Procedure to estimate geographical potentials per VRE asset.
Source: Authors' elaboration.

factors). Similarly, we also considered three cases (high, medium and low potentials) for offshore wind based on high, medium and low suitability factors.

2.2. Data processing task 2: Time series, mean and standard deviation per VRE asset

We used historical hourly meteorological reanalysis data during 2000–2015 from NASA's Modern Era Retrospective-Analysis for Research and Applications (MERRA) database (NASA, 2019) to determine the hourly CF time series, including its mean and standard deviation. We extracted hourly wind speed and solar irradiance data for each grid cell from the MERRA database. Sections 2.2.1 and 2.2.2 respectively describes how they were converted into the CF time series for wind and PV.

2.2.1. Wind

Following a three-step approach (see Fig. 4), we determined the CF time series for both onshore wind and offshore wind.

- **Step 1. Determine wind speed at turbine height**

Based on their eastward (m) and northward components (n), we calculated the hourly wind speed (v) at 2 m and 10 m above displacement height (d) and at 50 m above ground:

$$v = \sqrt{m^2 + n^2} \tag{3}$$

Using logarithmic law, wind speed at any height z (v_z) can be extrapolated from the surface roughness length z_0 and a known wind speed at reference height z_{ref} above ground (v_{ref}) [61].

$$v_z = v_{ref} \frac{\ln(\frac{z-d}{z_0})}{\ln(\frac{z_{ref}-d}{z_0})} \tag{4}$$

z_0 was determined through a linear regression using the 16-year time series of wind speed at 2 m and 10 m above displacement height (v_{2+d} andv_{10+d}) for each grid cell:

$$v_{2+d} ln10 - v_{10+d} ln2 = ln z_0 (v_{10+d} - v_{2+d}) \tag{5}$$

We then calculated the 16-year-average wind speed at 100 m above displacement height (v_{100+d}) using formula (4). The International Electrotechnical Commission (IEC)'s 61400-12-1 international standards [54] classify wind turbines based on the local average wind speed at turbine hub height. In absence of manufacturer specifications of hub height, we used v_{100+d} as the basis to pre-select the turbine class most suitable to the local wind conditions per grid cell. Following Zappa and Van den Broek [62], we adopted three representative onshore turbine modules and one offshore turbine module from the Danish manufacturer Vestas. Table 4 presents the four Vestas modules in relation to the IEC's classification and their key technical parameters. Note that the hub height (h_{hub}) was estimated based on its empirical relationship with rotor diameter (D) [63]:

$$h_{hub} = 2.7936 D^{0.7663} \tag{6}$$

- **Step 2. Determine hourly CF at sea level**

After the selection of most suitable turbine module for each grid cell, the time series of hourly wind speed at hub height were calculated. This enabled us to determine the time series of hourly CF using the power curves of the four individual turbine modules specified by the manufacturer[5]. Fig. 5 presents these power curves. Because the power curves are tested at sea level with a reference air density (ρ_0 = 1.225kg/m^3), the determined CF only reflects the hourly power output per unit rated power at sea level [42]. They must be corrected for the average elevation of suitable area (h) in each grid cell to take reduced air density into account.

- **Step 3. Determine hourly CF at elevation level and its mean and standard deviation**

Following Eurek et al. [42], we developed an approach to obtain the hourly CF time series, adjusted for elevation. For any elevation level h, a new power curve of a specific turbine module can be constructed from its original power curve at sea level. This was achieved through

[5] Note that we do not explicitly consider the "memory effect" of wind speed propagation within a wind farm and the wind farm wake effect. The former can smooth the aggregated power curve of multiple turbines [27]. The latter causes power losses and thus affects the aggregated power curve as well [64].

Table 2
Geographical constraints for determining available area for VRE development.
Source: Compiled based on Global Administrative Area [40], Flanders Marine Institute [41], Eurek et al. [42], British Oceanographic Data Centre [43], Peyrard [44], Halpern et al. [45], Bosch et al. [46], Mahlknecht [47], International Union for the Conservation of Nature and United Nations Environment Programme [48], Gruber [49], United States Geological Survey [50], and Sun et al. [37].

Constraint for each VRE technology	Data sources	Onshore wind	Offshore wind	Utility-PV	Rooftop PV
Territory (km^2)	GADM Database of Global Administrative Areas [40]; Maritime Boundaries Geodatabase [41]	Administrative terrestrial area	Economical exclusive zone	Administrative terrestrial area	Administrative terrestrial area
Distance to shore (km)	NA	NA	10–90 Note following Eurek et al. [42], we set the minimum distance to shore at ~10 km to restrict the visibility and environmental impacts of offshore wind. We also considered distance to shore above 90 km too far to develop offshore wind.	NA	NA
Depth (m)	General bathymetric chart of the oceans (GEBCO)_2014 (British Oceanographic Data [43]	NA	≤60 We only considered offshore wind turbines with bottom fixed foundations (no floating), which usually suit water depth below 60 m [44]	NA	NA
Commercial maritime transport (annual number of ship tracks per square km^2 in 2013)	Cumulative human impacts: raw stressor data of 2013 commercial shipping activities [45]	NA	≤25	NA	NA
Submarine communications cable	Greg's Cable Map of undersea cable initiatives [47]	NA	1 km^2 buffering from both sides of the cable [46]	NA	NA
Protected areas (km^2)	The world database on protected areas (WDPA) and Marine Protected Areas (International Union for the Conservation of Nature and United Nations Environment Programme, 2017)	Terrestrial protected areas	Terrestrial & maritime protected areas	Terrestrial protected areas	Terrestrial protected areas
Permafrost (%)	Global Permafrost Zonation Index Map [49]	≤0.1	NA	≤0.01	≤0.01
Elevation (m)	Digital Elevation - Global 30 Arc-Second Elevation (GTOPO30) [50]	< =2600 Note Eurek et al. [42] considered elevation above 2500 m too high for onshore wind development due to substantial reduction of wind power density associated air density losses. However, we set the threshold elevation at 2600 m, because wind farms above 2600 m have been accomplished in China.	NA	NA	NA
Slope (degree)	Calculated based on Elevation	< 11.31 (or 20%) [42]	NA	< 4 (or 6.99%) [37]	NA

Table 3
Suitability factors for different land cover categories.[a]
Source: Complied based on Bontemps et al. [51], Hoogwijk [52], Herran et al. [38], Eurek et al. [42], Sun et al. [37], and Deng et al. [53].

GlobCover code	GlobCover Category	Suitability factor							
		Onshore wind (High)	Onshore wind (Medium)	Onshore wind (Low)	Utility-PV	Rooftop PV	Offshore wind (High)	Offshore wind (Medium)	Offshore wind (Low)
11	Post-flooding or irrigated croplands	0	0	0.00	0	0	0	0	0
14	Rainfed croplands	0.70	0.60	0.30	0.01	0	0	0	0
20	Mosaic Cropland (50%-70%)/ Vegetation (grassland, shrubland, forest) (20–50%)	0.70	0.60	0.30	0.01	0	0	0	0
30	Mosaic Vegetation (grassland, shrubland, forest) (50–70%)/Cropland (20–50%)	0.70	0.50	0.20	0.01	0	0	0	0
40	Closed to open (> 15%) broadleaved evergreen and/or semi-deciduous forest (> 5m)	0.10	0	0	0	0	0	0	0
50	Closed (> 40%) broadleaved deciduous forest (> 5m)	0.10	0	0	0	0	0	0	0
60	Open (15–40%) broadleaved deciduous forest (> 5m)	0.10	0	0	0	0	0	0	0
70	Closed (> 40%) needle leaved evergreen forest (> 5m)	0.10	0	0	0	0	0	0	0
90	Open (15–40%) needle leaved deciduous or evergreen forest (> 5m)	0.10	0	0	0	0	0	0	0
100	Closed to open (> 15%) mixed broadleaved and needle leaved forest (> 5m)	0.10	0	0	0	0	0	0	0
110	Mosaic Forest/Shrubland (50–70%)/Grassland (20–50%)	0.50	0.36	0.14	0.01	0	0	0	0
120	Mosaic Grassland (50–70%)/Forest/Shrubland (20–50%)	0.65	0.46	0.19	0.05	0	0	0	0
130	Closed to open (> 15%) shrubland (< 5m)	0.50	0.36	0.14	0.01	0	0	0	0
140	Closed to open (> 15%) grassland	0.80	0.57	0.23	0.01	0	0	0	0
150	Sparse (> 15%) vegetation (woody vegetation, shrubs, grassland)	0.90	0.50	0.10	0.01	0	0	0	0
160	Closed (> 40%) broadleaved forest regularly flooded - Fresh water	0	0	0	0	0	0	0	0
170	Closed (> 40%) broadleaved semi-deciduous and/or evergreen forest regularly flooded - Saline water	0	0	0	0	0	0	0	0
180	Closed to open (> 15%) vegetation (grassland, shrubland, woody vegetation) on regularly flooded or waterlogged soil - Fresh, brackish or saline water	0	0	0	0	0	0	0	0
190	Artificial surfaces and associated areas (urban areas > 50%)	0	0	0	0	0.07	0	0	0
200	Bare areas	0.90	0.50	0.10	0.05	0	0	0	0
210	Water bodies	0	0	0	0	0	0	0	0
220	Permanent snow and ice	0	0	0	0	0	0	0	0
*	Sea (10 km < =distance to shore < =90 km and depth < =60 m)	0	0	0	0	0	0.5	0.4	0.3

[a] The land cover categories and corresponding codes are based on GlobCover 2009V2.3 Global Land Cover Map [51]. Suitability factors for onshore wind and utility-PV are compiled from Hoogwijk [52], Herran et al. [38], Eurek et al. [42]. Following Sun et al. [37], we limited the deployment of rooftop PV to built-up areas (i.e. artificial surfaces and associated areas under the GlobCover Category). The suitability factor of 0.07 for rooftop PV is the product of the assumed roof area per built-up area (0.15–0.3) and the popularizing ratio of rooftop PV (0.3) [37]. We also added a land cover category "Sea" with code * specially for offshore wind. The suitability factors for offshore wind from the available sea area here are set at 0.5, 0.4 and 0.3 as high, medium and low values. This is comparable to Deng et al. [53], where suitability factors of 0.1, 0.3 and 0.4 are assumed for offshore wind.

Table 4
Vestas turbine modules and their key technical parameters.
Sources: IEC [54]; Wind-turbine-models.com [55–58].

IEC's wind turbine classification according to average wind speed	Usage	Representative commercial turbine module	Rated capacity (MW)	Rotor diameter (m)	Specific power (W/m^2)	Cut-in speed (m/s)	Rated speed (m/s)	Cut-off speed (m/s)	Estimated hub height (m)
Class I: 10 m/s	Onshore	Vestas 105–3.3	3.3	105	381.8	3	13	25	99
Class II: 8.5 m/s	Onshore	Vestas 117–3.3	3.3	117	306.9	3	13	25	107
Class III: 7.5 m/s	Onshore	Vestas 126–3.3	3.3	126	264.7	3	12	22.5	114
Class S: User defined	Offshore	Vestas 164–8.0	8	164	378.7	4	13	25	139

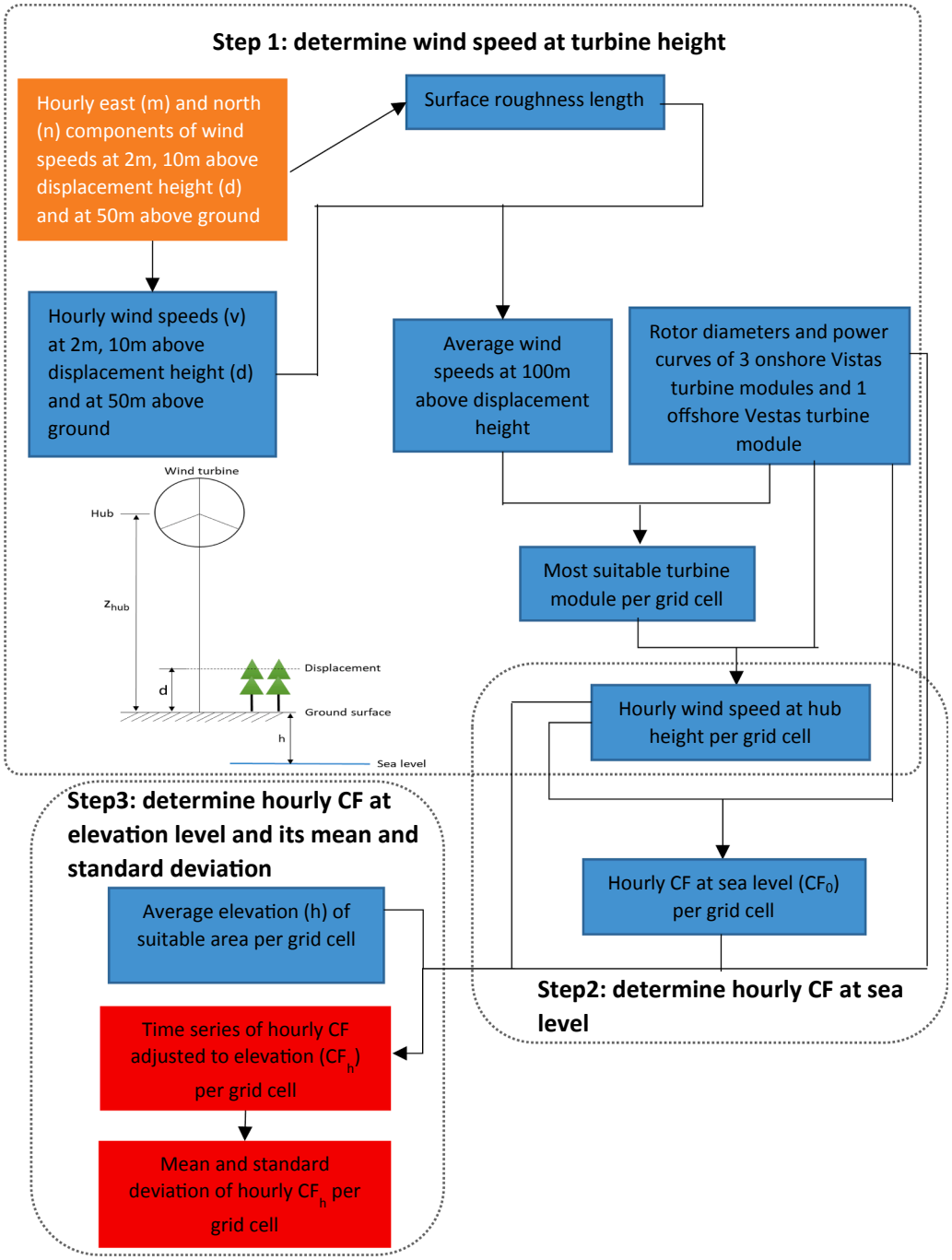

Fig. 4. Method to determine the hourly CF time series for onshore and offshore wind. Source: Authors' elaboration.

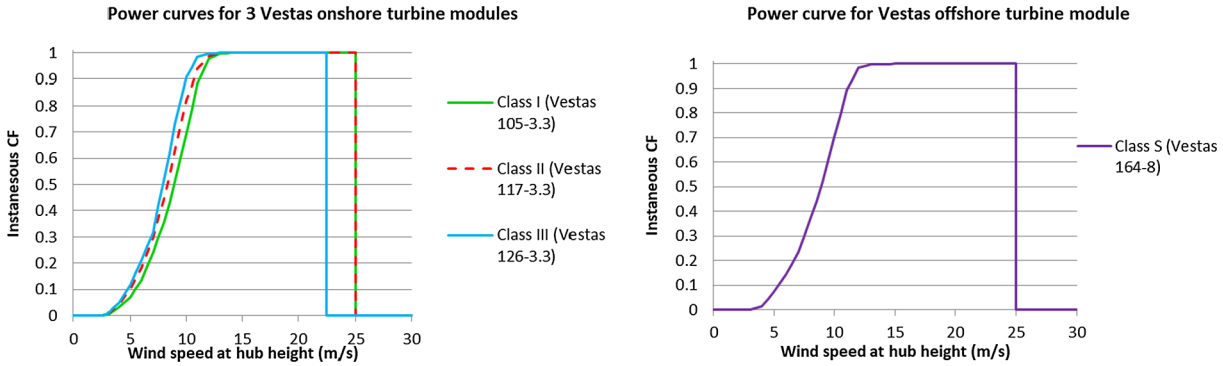

Fig. 5. Power curves for four Vestas turbine modules.
Source: Wind-turbine-models.com [55–58].

dividing the new power curve into five intervals, using the cut-in speed (v_{in}), the rated wind speed at sea level (v^0_{rated}), the rated wind speed at elevation level (v^h_{rated}) and the cut-off speed (v_{off}). v_{in}, v^0_{rated} and v_{off} are all specified in the original power curve, while v^h_{rated} can be estimated from v^0_{rated}.

At a wind speed between v_{in} and v^0_{rated}, the instantaneous CF for a turbine with sweeping area (A) and rated power (P_{rated}) at a given air density (ρ) and power coefficient[6] (C_p) is

$$CF = \frac{1}{2} C_p \rho A v^3 / P_{rated} \tag{7}$$

In this case, CF is proportionated to ρ, ceteris paribus. Assuming negligible impacts of temperature and pressure, air density at a specific h (ρ_h) can be estimated based on a simple linear relationship [42]:

$$\rho_h = 1.225 - 1.194 * 10^{-4} h, \tag{8}$$

or

$$\frac{\rho_h}{\rho_0} = 1 - 0.975 * 10^{-4} h \tag{9}$$

According to Eurek et al. [42], for the same turbine module, the equivalent wind speed (v_h) at elevation h that results in the same CF from a wind speed at sea level (v_0) can be calculated via

$$v_h = \left(\frac{\rho_h}{\rho_0}\right)^{-1/\varepsilon} v_0 \tag{10}$$

Here ε is used to correct for the non-constant C_p at different wind speeds. If C_p is assumed to be constant, ε is 3. Without the assumption of constant C_p, parameter ε approximates 1.5 in case that the wind speed is above 12 m/s [42,68]. As v^0_{rated} for all four turbine modules are above 12 m/s, we estimated v^h_{rated} via the following formula:

$$v^h_{\text{rated}} = \left(\frac{\rho_h}{\rho_0}\right)^{-2/3} v^0_{\text{rated}} \tag{11}$$

Consequently, we determined CF at elevation h (CF_h) from CF at sea level (CF_0), based on the five intervals divided from the new power curve. If the wind speed (v) is below v_{cut-in}, CF_h is 0; if v is between v_{in} and v^0_{rated}, $CF_h$is the product of CF_h and the ratio $\frac{\rho_h}{\rho_0}$; if v is above v^h_{rated} but below v_{off}, $CF_h$is 1; if v is between v^0_{rated} andv^h_{rated}, CF_h is linearly interpolated; if v is above v_{off}, CF_h is 0. This creates a stepwise function:

$$CF_h = \begin{cases} CF_h = 0, & \text{if } v < v_{in} \\ CF_0 \frac{\rho_h}{\rho_0} = CF_0 * (1 - 0.975 * 10^{-4} h), & \text{if } v_{in} \le v \le v^0_{rated} \\ 1 - 0.975 * 10^{-4} h + \frac{0.975 * 10^{-4} h}{v^h_{rated} - v^0_{rated}} (v - v^0_{rated}), & \text{if } v^0_{rated} < v < v^h_{rated} \\ 1, & \text{if } v^h_{rated} \le v < v_{off} \\ 0, & \text{if } v \ge v_{off} \end{cases} \tag{12}$$

For illustration purpose, the power curves for a class III turbine module at sea level and adjusted to elevation at 2000 m are presented in Fig. 6.

The mean (μ) and standard deviation (σ) of the 16-year (140256-hour) time series of hourly CF_h corrected for elevation were determined for each grid cell via:

$$\mu = \frac{\sum_{t=1}^{140256} CF_{h,t}}{140256} \tag{13}$$

$$\sigma = \sqrt{\frac{\sum_{t=1}^{140256} (CF_{h,t} - \mu)^2}{140256}} \tag{14}$$

2.2.2. Solar PV

Fig. 7 shows a four-step approach to determine the hour CF time series for both utility-PV and rooftop PV.

- **Step 1: Calculate apparent solar time (AST) and solar angles**

AST and solar angles depend on local geographical coordinates (longitude and latitude) of each grid cell and the local standard time (LST). The LST is set as the middle point of each hour in the time series. For China, AST was calculated via

$$AST = LST + ET + 4(SL - LL) - DS\,[hour] \tag{15}$$

$$ET = 9.87 sin(2B) - 7.53 cos(B) - 1.5 sin(B)\,[min] \tag{16}$$

$$B = \frac{(N - 81)360}{364} \tag{17}$$

where ET is equation of time; SL is standard longitude; LL is local longitude; DS is day-light saving time (which is zero for China); N is the day number of the year [69].

Although SL is normally the standard meridian (every multiple of 15°) for dividing standard time zones, China only has one official national standard time (China Standard Time) based on SL at 120°.

Solar altitude angle (α) and azimuth angle (Z_s) were calculated through

$$sin(\alpha) = sin(L) sin(\delta) + cos(L) cos(\delta) cos(H) \tag{18}$$

$$\alpha = arcsin(\alpha) \tag{19}$$

[6] The power coefficient is the ratio of the power captured by the turbine rotor divided by the total power available in the wind [65]. It is a function of wind speed and capped by the Betz's limit at 0.593 [66,67].

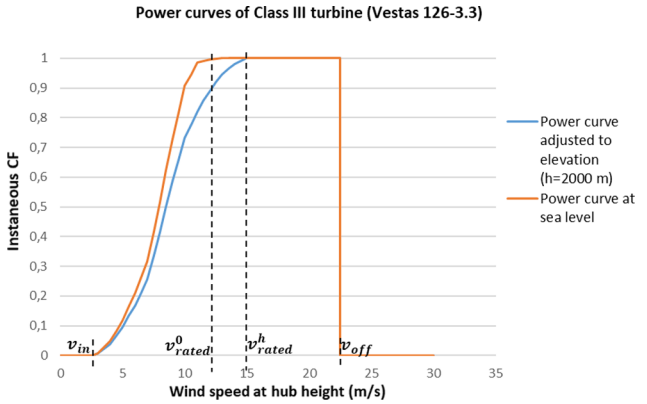

Fig. 6. Power curves of Class III wind turbine at sea level and corrected for elevation.
Source: Authors' elaboration.

$$\delta = 23.45sin(\frac{360(284+N)}{365}) \quad (20)$$

$$H = (AST - 12)15 \quad (21)$$

$$cos(Z_s) = \frac{\cos(\delta)(\cos(L)\tan(\delta) - \sin(L)\cos(H))}{\cos(\alpha)} \quad (22)$$

$$Z_s = \begin{cases} arccos(Z_s), \ ifH < 0 \\ 360 - arccos(Z_s), \ ifH > 0 \end{cases} \quad (23)$$

where L is local latitude; δ is declination angle; H is hour angle (Muneer et al., 2004; [69]).

- **Step 2: Estimate the diffuse and direct fractions of global horizontal irradiance**

To determine the diffuse and direct components of hourly global horizontal irradiance, we used Boland–Ridley–Lauret (BRL) model to

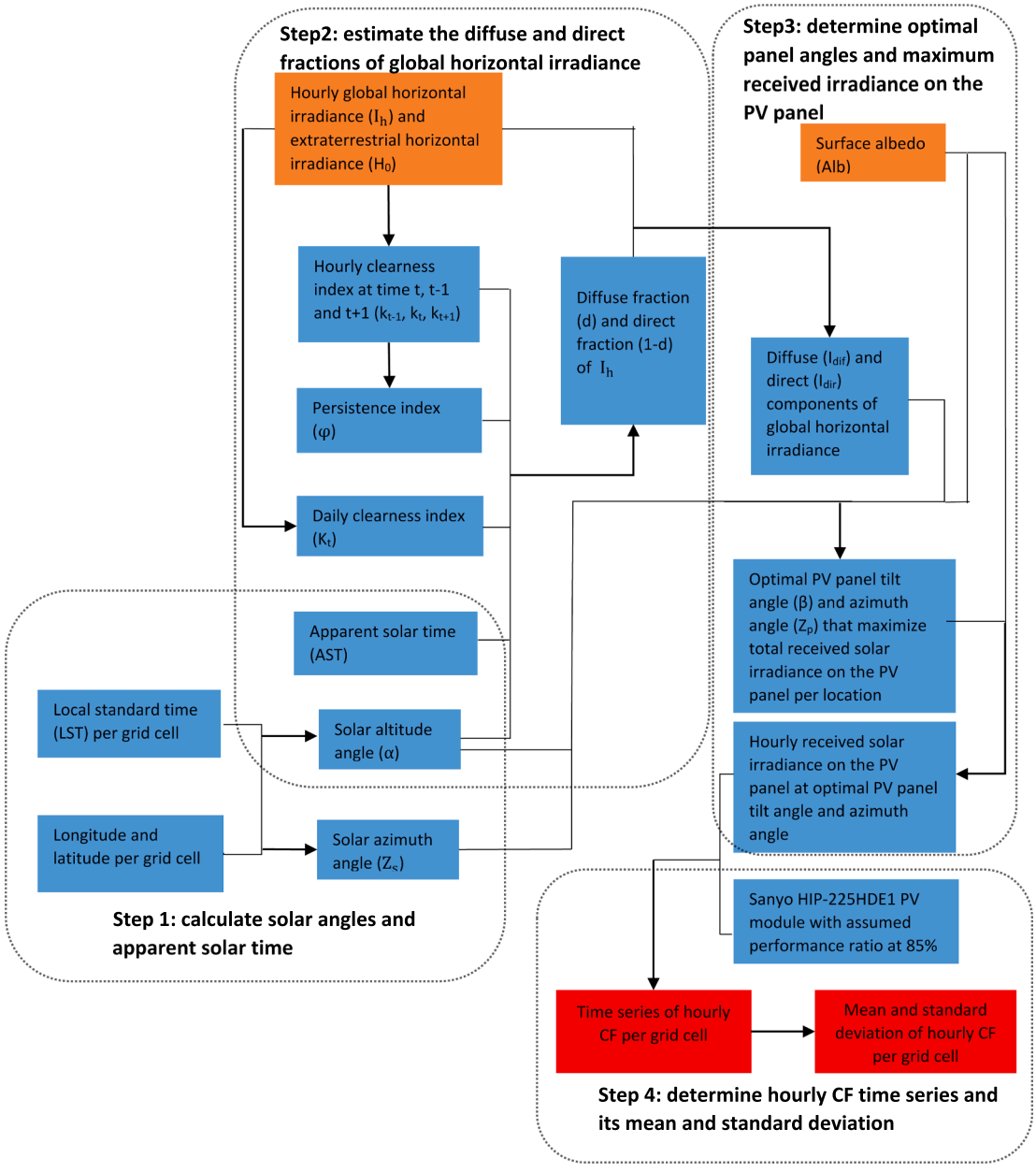

Fig. 7. Method to determine the hourly CF time series for utility-PV and rooftop PV.
Source: Authors' elaboration.

estimate the hourly diffuse fraction (df). The BRL model is multi-variable logistic model based on hourly global horizontal irradiance (I_h) and extraterrestrial horizontal irradiance (H_0)[7] [70]:

$$df = \frac{1}{1 + exp(-5.38 + 6.63k_t + 0.006AST - 0.007\alpha + 1.75K_t + 1.31\varphi)} \quad (24)$$

$$k_t = \frac{I_{h,t}}{H_{0,t}} \quad (25)$$

$$K_t = \frac{\sum_{t=0}^{23} I_{h,t}}{\sum_{t=0}^{23} H_{0,t}} \quad (26)$$

$$\varphi = \begin{cases} \frac{1}{2}(k_{t-1} + k_{t+1}), & if \quad t_{sunrise} < t < t_{sunset} \\ k_{t-1}, & if \quad t = t_{sunrise} \\ k_{t+1}, & if \quad t = t_{sunset} \end{cases} \quad (27)$$

where k_t, K_t and φ are respectively hourly clearness index, daily clearness index and persistence index.

The hourly diffuse ($I_{dif,h}$) and direct ($I_{dir,h}$) components of I_h are:

$$I_{dif,h} = dfI_h \quad (28)$$

$$I_{dif,h} = (1 - df)I_h \quad (29)$$

- **Step 3: Determine optimal panel angles and maximum received irradiance on the PV panel**

The hourly total received irradiance on the PV panel (I_p) consists of direct ($I_{dir,p}$), diffuse ($I_{dif,p}$) and reflection ($I_{r,p}$) components:

$$I_p = I_{dir,p} + I_{dif,p} + I_{r,p} \quad (30)$$

Depending on the panel tilt angle (β) and azimuth angle (Z_p), the three irradiance components can be determined via:

$$I_{dir,p} = \frac{I_{dir,h}\cos(\theta)}{cos(90 - \alpha)} \quad (31)$$

$$cos(\theta) = sin(\alpha)cos(\beta) + cos(\alpha)sin(\beta)cos(Z_p - Z_s) \quad (32)$$

$$I_{dif,p} = \frac{1 + cos\beta}{2} I_{dif,h} \quad (33)$$

$$I_{r,p} = \frac{1 - cos\beta}{2}(I_{dir,h} + I_{dif,h})Alb \quad (34)$$

where θ is incidence angle; Alb is surface albedo [71].

Based on $I_{dif,h}$ and $I_{dir,h}$, we determined the optimal panel tilt angle (β) and azimuth angle (Z_p) to maximize the annual total irradiance received on the PV panel. The same optimal angles apply for both utility-PV and rooftop PV, since we assumed utility-PV and rooftop PV are mounted on a surface close to flat (ground with slope below 4° or flat roof). The optimization was performed on an annual basis for each grid cell. In the optimization process we filtered out irradiances associated with α smaller than 0.1°, because very small α can drastically inflate the total received irradiance. The final angles adopted were calculated from the 16-year average value of the optimized angles, based on which we obtain the time series of hourly irradiance received on the PV panel.

- **Step 4. Determine hourly CF time series and its mean and standard deviation**

The power conversion performance of the selected Sanyo HIP-225HDE1 module is relatively less dependent on temperature [72]. Thus, we assumed a uniform performance ratio (PR) at 85% across all grid cells to correct for efficiency losses at non-standard test conditions. This value might seem optimistic, but can be considered realistic even today[8]. The hour CF was determined through

$$CF = \frac{I_p}{I_{STC}} PR \quad (35)$$

Where I_{STC} is solar irradiance under standard test conditions, which is 1000 W/m^2.

Note that within the same grid cell, both utility-PV and rooftop PV have identical 16-year time series profile of hourly CF since the same PV module and optimal panel angles were used. Consequently, we determined the mean (μ) and standard deviation (σ) of hourly CF time series per grid cell using formula (13) and (14).

2.3. Data processing task 3: Potentials-weighted average CF per VRE technology

Based on the 16-year mean CF characterized for each VRE technology per grid cell, we calculated the average CF (weighted by potentials per grid cell) for each VRE technology in China:

$$\bar{CF}_j = \sum_i \mu_{j,i} \frac{P_{j,i}}{P_j}, j = onshore \quad wind, \quad offshore \quad wind, \quad utility\_PV, \quad rooftop \quad PV \quad (36)$$

where $\bar{CF}_j$ is the average CF for technology j in China; $\mu_{j,i}$ is the mean CF for technology j in grid cell i; $P_{j,i}$ is potentials for technology j in grid i; P_j is total potentials for technology j in China.

2.4. Data processing task 4: LCOE per VRE asset

The LCOE for each VRE asset was calculated via:

$$\mathrm{LCOE}_k = \mathrm{LCOE}_{j,i} = \frac{a \cdot I_j + O\&M_j}{8760\mu_{j,i}}, \quad (37)$$

$$a = \frac{r}{1 - (1 + r)^{-L}} \quad (38)$$

where LCOE_k is LCOE for VRE asset k of technology j in grid cell i; I_j is capital costs and $O\&M_j$ is annual fixed operating and maintenance (O&M) costs for technology j; $\mu_{j,i}$ is the mean CF for technology j in grid cell I; r is the discount rate; a is the capital recovery factor.

We set r as the social discount rate at 4%. The unit capital costs and O&M costs for each VRE technology were adopted from the IEA World Energy Outlook's 450 ppm scenario projected for the year 2040 (see Table 5). We presumed these costs are constant until 2050[9].

Uniform cost parameters were assumed for onshore wind, utility-PV and rooftop PV across different grid cells. While for offshore wind we used scaling factors to take into account the impact of different average distances to shore and depths on capital costs. Fig. 8 shows the capital costs scaling factors for offshore wind, where costs in Table 5 (2450 USD$_{2015}$/kW) were used as a reference case (with unity scaling factor).

Consequently, we scaled up the capital costs for offshore wind in each grid cell:

$$I_{offshore,i} = 2450SF_i \quad (39)$$

where $I_{offshore,i}$ is the capital costs scaled up for offshore wind in grid cell i and SF_i is the scaling factor for grid cell i.

[7] Global horizontal irradiance and extraterrestrial horizontal irradiance sometimes are also referred to as "terrestrial horizontal irradiance" and "clear-sky horizontal irradiance", respectively. The former refers to solar irradiance received on a horizontal plane on earth, while the latter refers to solar irradiance received outside the atmosphere.

[8] Reich et al. [73] found that the median measured PR for 100 PV installations is ~84% in 2010. They further conclude that an above-90% PR is even realistic back in 2010 and it would be more common in the future.

[9] Note this might lead to overestimated costs if the trend of technological learning continues.

Table 5
Unit costs assumptions for each VRE technology in 2050.
Source: IEA [74].

VRE technology	Capital costs (USD_{2015}/kW)	Fixed O&M costs (USD_{2015}/kW)
Onshore wind	1160	30
Offshore wind	2450	100
Utility-PV	680	12
Rooftop PV	760	12

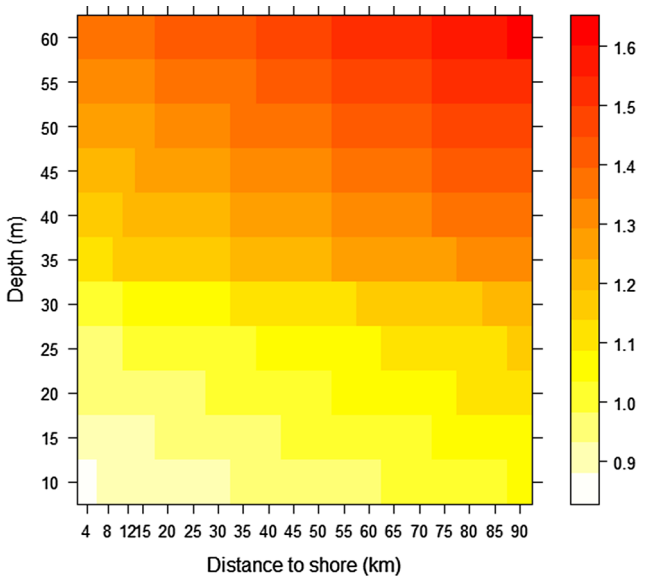

Fig. 8. Capital costs scaling factors for offshore wind (Klinge Jacobsen et al. [75] developed scaling factors for depth and distance to shore up to 35 m and 25 km, respectively. We calibrated them to IEA's costs prediction to use the latter as reference case. For depth beyond 35 m, we assumed the scaling factors are mainly driven by costs increase of the jacket, the most cost-effective turbine foundation. Based on ECN's foundation costs model [76] in relation to depth, we extended the scaling factors to depths up to 60 m. For distance to shore between 25 km and 90 km, we used linear extrapolation to develop the scaling factors.).
Source: developed and calibrated based on IEA [74], Klinge Jacobsen et al. [75], and Lensink [76].

2.5. Data processing task 5: MPT optimization

Based on the hourly CF time series obtained for each VRE asset (see Section 2.2), we calculated the covariance matrix (**cov**) between different VRE assets. VRE assets with zero potentials were excluded to save computation time. To avoid co-linearity issues (due to identical CF time series in the same grid cell), we combined utility-PV and rooftop PV as the same VRE technology, i.e. "solar". This resulted in 3439 VRE assets and a 3439×3439 **cov**. We then performed the MPT optimization analysis for three 2050 scenarios of high renewables in China to obtain the efficient frontier. These are the 1.5 °C Scenario, based on China' official Integrated Policy Assessment Model (IPAC) [35], Greenpeace's Energy Revolution scenario [77] and World Wildlife Fund (WWF)'s High Renewables scenario [62,78]. Key statistics of the three scenarios are presented in Table 6.

Then we performed the MPT optimization. We used the total installed VRE capacity prescribed by the three scenarios as sole budget constraints in the optimization to obtain the efficient frontier for wind-only portfolios, solar-only portfolios, and wind & solar portfolios with unconstrained shares of each VRE technology. The resulting portfolios are referred to as **portfolios with unconstrained shares.** After that, the optimization was performed again to obtain the efficient frontier for wind & solar portfolios with constrained shares of each VRE technology, as prescribed by the three scenarios. They are referred to as **portfolios with constrained shares**.

The MPT optimization aims to minimize the portfolio volatility (mimicked by the standard deviation of portfolio CF) for each portfolio return (mimicked by the mean portfolio CF). The portfolio return (μ_P) and volatility (σ_P) can be calculated as follows:

$$\mu_P = \sum_k \omega_k \mu_k = \mu^{\mathbf{T}} \omega \tag{40}$$

$$\sigma_P^2 = \sum_k \sum_m \omega_k \omega_m cov_{k,m} = \omega^{\mathbf{T}} \mathbf{cov} \omega \tag{41}$$

Where ω_k is contributing weight per VRE asset k (share of VRE asset k in total portfolio capacity); μ_k is 16-year mean CF for VRE asset k (see Section 2.2); $cov_{k,m}$ is the CF covariance between assets k and m; $\mu^{\mathbf{T}}$ is the transpose vector of mean CF; $\omega^{\mathbf{T}}$ and ω are respectively the transpose vector and vector of contributing weight; **cov** is the covariance matrix.

We formulated the MPT optimization as a constrained programming problem, based on the copperplate assumption. Thus, transmission constraints in terms of existing or planned transmission grids were not factored into the optimization. The optimization followed three steps. Firstly, we identified the maximum return portfolio (referred to as **maxret portfolio**) positioned on the efficient frontier through linear programming:

$$\max_{\omega_k} \mu_P$$

$$\text{subjectto: } \begin{cases} \sum_k \omega_k = 1 \\ \omega_k \le \frac{P_k}{C} \\ \sum_{k \in j} \omega_k = \frac{C_j}{C} (constrained \quad shares) \end{cases} \tag{42}$$

Table 6
Key statistics of three high renewables scenarios for China in 2050.
Source: (a) Jiang et al. [35]; (b) Greenpeace, Global Wind Energy Council (GWEC) and SolarPower Europe (2015); (c) WWF [58,78].

Scenario		IPAC 1.5 °C Scenario[a]	Greenpeace Energy Revolution Scenario[b]	WWF High Renewables Scenario[c]
Renewables penetration in demand (%)		59*	88	88
VRE penetration in demand (%)		38*	55	62
Total installed VRE capacity (GW)		3732	2413	3210
Installed wind (GW)		1486	1181	1710
Of which	Onshore wind (GW)	NA	972	1455
	Offshore wind (GW)	NA	209	255
Installed Solar (GW)		2246	1232	1500
Share of wind in total installed VRE capacity (%)		40	49	53
Of which	Onshore wind (%)	NA	40	45
	Offshore wind (%)	NA	9	8
Share of solar PV in total installed VRE capacity (%)		60	51	47

* In absence of demand data, VRE penetration was calculated based on electricity generation.

where C is total installed VRE capacity.

It is subject to two constraints: the sum of the contributing weights of all VRE assets is equal to one, and the contributing weights of VRE asset k must not exceed its potentials' share in total installed VRE capacity ($\frac{P_k}{C}$). Note that the medium potentials for onshore wind and offshore wind assets (see Section 2.1.2) were used to formulate the constraint. For portfolios with constrained shares, the sum of the contributing weights of assets belonging to technology j must equal the required share of technology j in total installed capacity ($\frac{C_j}{C}$).

Secondly, we found the minimum volatility portfolio (referred to as **minvol portfolio**) along the efficient frontier based on quadratic programming (using the same constraints as in the linear programming formulated before).

$$\min_{\omega_k} \sigma_P^2$$

$$\text{subjectto: } \begin{cases} \sum_k \omega_k = 1 \\ \omega_k \le \frac{P_k}{C} \\ \sum_{k\in j} \omega_k = \frac{C_j}{C}(constrained \quad shares) \end{cases} \tag{43}$$

Lastly, based on returns associated with the minvol portfolio and maxret portfolio, we divided the return range in between in and 50 equal-distanced return points. We then performed the quadratic programming again to minimize the volatility for each of these return points. This naturally depicted the entire efficient frontier.

2.6. Post-processing task 1: Spatial distribution of contributing weights for selected portfolios

To enable comparison, we analysed the spatial distribution of contributing weights for the minvol portfolio, the portfolio with minimum coefficient of variation (CV)[10] (referred to as **minCV portfolio**), and the maxret portflio positioned on the efficient frontier. The analysis was performed for both portfolios with unconstrained and constrained technology shares (see Section 2.5).

2.7. Post-processing task 2: Portfolio share per VRE technology

Based on contributing weights of each VRE asset, we calculated the portfolio share per VRE technology for wind & solar portfolios with unconstrained technology shares (where the total installed VRE capacity serves as the sole budget constraint):

$$\omega_j = \sum_{k\in j} \omega_k \tag{44}$$

We compared the portfolio share per VRE technology between different scenarios. We also assessed the difference between the calculated unconstrained shares and the pre-defined constrained technology shares.

2.8. Post-processing task 3: Portfolio LCOE

We calculated the portfolio LCOE via

$$\text{LCOE}_p = \frac{\sum_k LCOE_k \omega_k \mu_k}{\mu_P} \tag{45}$$

Where LCOE_p is the portfolio LCOE; $LCOE_k$ (see Section 2.4) ω_k and μ_k are respectively the LCOE, contributing weight and mean CF of VRE asset k; μ_P is the portfolio return.

Since we combined utility-PV and rooftop PV as solar, the LCOE associated with each solar asset was calculated as the average LCOE weighted by the potentials of utility-PV and rooftop PV in the same grid cell.

2.9. Post-processing task 4: Portfolio CF duration curve and CF-at-risk

Based on contributing weights and the CF time series of each VRE asset (see Section 2.2), we determined the 16-year time series of the portfolio hourly CF:

$$\text{CF}_{p,t} = \sum_k \omega_k CF_{k,t} \tag{46}$$

Following Shahriari and Blumsack [23], we plotted the long-time duration curve of portfolio CF in relation to its availability (i.e. percentage of time), based on the 16-year time series of hourly portfolio CF. From the portfolio CF duration curve, we obtained the long-time CF-at-risk at 100% and 90% availability of time (denoted respectively as $\mathbf{CF_{100\%}}$ and $\mathbf{CF_{90\%}}$). These values represent the minimum CF that is available 100% and 90% of time[11]. After that, we determined the portfolios with the highest long-time $\text{CF}_{100\%}$ and $\text{CF}_{90\%}$ (referred to as $\mathbf{maxCF_{100\%}}$ **portfolio** and $\mathbf{maxCF_{90\%}}$ **portfolio**) positioned on the efficient frontier. To investigate the inter-annual variation of $\text{CF}_{100\%}$ and $\text{CF}_{90\%}$, we plotted the distribution of annual $\text{CF}_{100\%}$ and $\text{CF}_{90\%}$ for these portfolios together with the minvol portfolio, minCV portfolio and maxret portfolio. The sample data for the distribution were obtained from the annual CF duration curve of each individual year.

3. Results

3.1. Geographical potentials

3.1.1. Geographical potentials per VRE asset

Geographical potentials per VRE asset and their spatial distribution in China are shown in Fig. 9. Three cases are included (high, medium and low potentials, see Section 2.1.2) for onshore and offshore wind. As the figure shows, in all three cases, the geographical potentials for onshore wind are concentrated in North (including inner-Mongolia) and Northeast China. This is explained by the geographical constraints applied in the analysis. The exclusion of the 10 km distance from dense urban areas, in the medium case mainly reduces the onshore wind potentials in Northeast China compared to the high case, whereas the potentials in the low case are more evenly reduced over the grid cells by the use of low suitability factors. As for solar, its potentials are spread extensively over China except for Tibet, north Inner-Mongolia and the north of Northeast China due to the exclusion of sloped and permafrost areas. In particular, North and Northwest China have the largest geographical potentials for solar.

3.1.2. Total potentials per VRE technology

Total potentials for each VRE technology are presented in Table 7. China has huge potentials for solar, being 1.6 times larger than the high potentials case of onshore wind. The potential of offshore wind is relatively limited, also in the high potential case. The latter is explained by the relatively small sea area meeting the constraints of depth $\le$ 60 m and distance to share $\le$ 90 km. We consider the medium case for onshore and offshore wind as a reasonable estimate. If not specified, the results presented in the following sections are based on the medium potential case. For information purposes only, we also show the total potential annual electricity generation (in TWh) for each

[10] CV is the ratio between portfolio volatility and portfolio return. Therefore, the minimum CV portfolio is the point with the highest slope along the efficient frontier. This is referred to as the maximum Sharpe ratio portfolio in Shahriari and Blumsack [23].

[11] 90% is assumed to reflect the availability of coal-fired plants, the predominant power generation technology now in China [79]. Therefore $\text{CF}_{90\%}$ can be interpreted as the minimum CF provided by the VRE portfolios if they are used to replace coal.

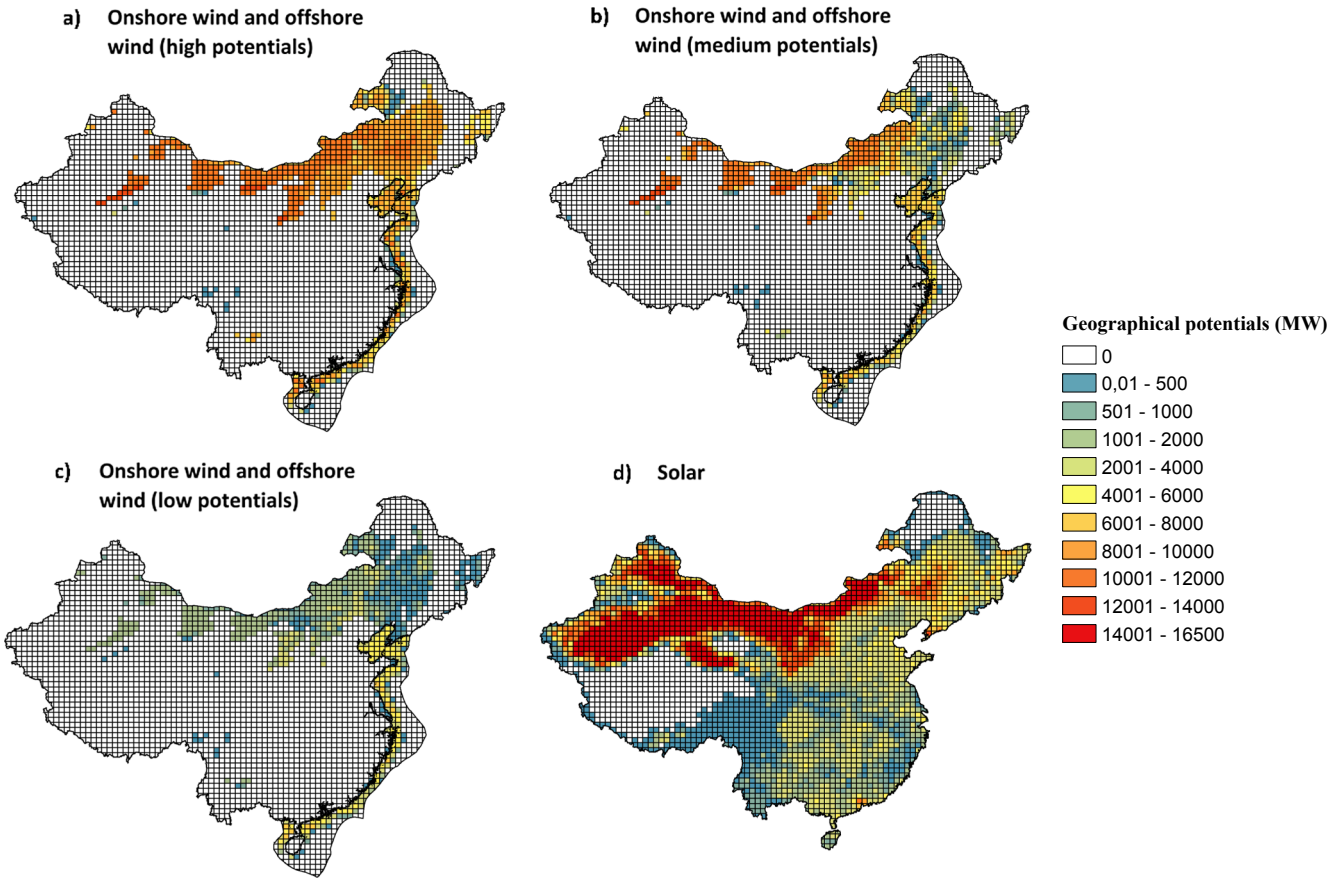

Fig. 9. Spatial distribution of geographical potentials per VRE asset in China (*zoom in for details*).
Source: Based on authors' analysis.

Table 7
Total potentials (in GW installed capacity) and potential annual electricity generation (in TWh) per VRE technology in China.
Source: Based on authors' analysis.

Technology	Onshore wind			Offshore wind			Solar			Total		
Geographical potentials (GW)	High	Medium	Low	High	Medium	Low	Total	Utility-PV	Rooftop PV	High	Medium	Low
	4909	3176	575	932	745	559	12,936	12,576	360	18,777	16,857	14,070
Potential annual electricity generation (TWh)	15,094	9654	1783	2776	2219	1665	23,570	23,025	580	41,440	35,443	27,018

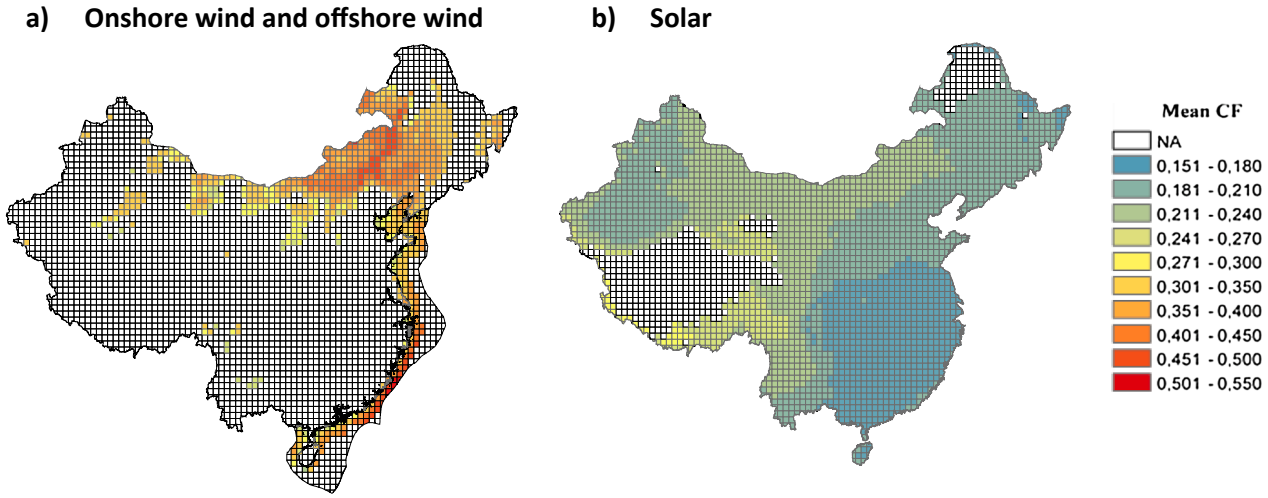

Fig. 10. Spatial distribution of mean CF per VRE asset in China.
Source: Based on authors' analysis.

technology[12] in Table 7. The calculation was based on the total potentials and the potential-weighted average CF (see Section 3.3).

3.2. Mean CF per VRE asset

Fig. 10 illustrates the mean CF per VRE asset in China. It shows that the assets with highest CF for onshore and offshore wind are located respectively in east Inner-Mongolia and the Taiwan Strait, where the mean CF can be above 40%. For solar, the best performing areas come from North and Southwest China, whereas South and East China have the lowest mean CF.

3.3. Potential-weighted average CF per VRE technology

The potential-weighted average CF for each technology is shown in Table 8. To enable comparison, we also give the minimum and maximum mean CF of individual asset. The average CF for onshore wind in China is 0.347, which is comparable to the global average CF from operating wind projects in 2017 [81]. Offshore wind has an almost identical average CF to onshore wind. This can be explained by the superior performance and abundant potentials of onshore wind located in Inner-Mongolia. By contrast, the potentials of best-performing offshore wind (around the Taiwan Strait) are relatively small, meaning that the average CF is dominated by less performing offshore wind assets. The average CF for utility-PV is slightly higher (~2 percentage point) than that for rooftop PV.

3.4. LCOE per VRE asset

The scatter plot of LCOE for each VRE asset (against its potentials in log scale) is illustrated in Fig. 11. It shows that the LCOE of onshore wind is slightly lower (between 25 and 45 USD_{2015}/MWh) than that of solar (between 25 and 55 USD_{2015}/MWh). By contrast, the LCOE for offshore wind varies widely between assets located in different grid cells, ranging between 63 and 145 USD_{2015}/MWh. The range in LCOE can be explained by the spatial distribution of LCOE for VRE assets (see Fig. 12). East Inner-Mongolia (onshore wind) and the Taiwan Strait (offshore wind) show the lowest LCOE, whereas the lowest LCOE for solar is in North and Southwest China. This outcome is consistent with the spatial distribution of the mean CF (see Section 3.2).

3.5. Efficient frontiers

Efficient frontiers generated from the MPT optimization are presented in Fig. 13. The three scenarios with different budgets of installed VRE capacity are indicated by different line types, while different colours are used to represent different portfolio types (wind-only, solar-only, wind & solar and wind & solar with constrained technology shares) within these scenarios. For comparison, we also show the return-volatility performance of individual VRE assets[13] (the dots in the figure). Both solar, onshore wind and offshore wind follow a clear tendency ("the higher the return, the higher the volatility"), although heteroscedasticity (unequal scatter) can be observed. The efficient frontiers for wind-only and solar-only portfolios demonstrate better return-volatility performance than individual wind and solar assets. Solar-only portfolios exhibit lower return but higher volatility than wind portfolios, mainly because of the diurnal pattern of solar generation. However, when solar assets mix with wind assets with unconstrained technology shares, their combined portfolios (the red lines) show the best return-volatility performance. Within the same scenario, not only does the wind & solar frontier cover a broader return range, but it shows a smaller volatility level at each attainable return level than the wind-only and solar-only frontiers. This finding is in agreement with Shahriari and Blumsack [23]. However, inferior return-volatility performance is observed for wind & solar portfolios with constrained technology shares (the green, orange and grey lines). For the same portfolio type (e.g. wind & solar), the efficient frontier within scenarios facing a higher capacity budget (e.g. 3732 GW within IPAC versus 2421 GW within Greenpeace) tends to show lower return-volatility performance, because more assets with inferior performance are needed.

3.6. Spatial distribution of contributing weights

Using the IPAC scenario, for example, we present the spatial distribution of contributing weights for the minvol (the minimum volatility), minCV (the minimum coefficient of variation) and maxret (the maximum return) portfolios positioned on the efficient frontier of wind & solar and wind & solar with constrained technology shares respectively in Figs. 14 and 15. The minvol, minCV and maxret portfolios sit on the bottom-left, steepest and top-right points of the efficient frontier, respectively.

In the minvol wind & solar portfolio with unconstrained technology shares (Fig. 14), onshore wind is mainly located in east Inner-Mongolia, Northeast, Northwest and North China, while solar is mainly located in Northeast, Northwest and East China. This shows the strong negative correlation between the power outputs of wind and solar assets in these regions. As portfolio return increases, solar assets are gradually replaced by wind assets due to the higher mean CF of the latter. This is true in the case of the minCV wind & solar portfolio, where solar assets in East China (with lowest mean CF) are mainly replaced by increased onshore wind assets in North China. As for the maxret wind & solar portfolio, contributing weights of onshore wind in North China reach the maximum. Solar assets nearly disappear, except for a few grid cells with very limited contributing weights in South Tibet. This is because solar assets in these grid cells have a higher mean CF than unused wind assets to meet the required capacity budget. Across all three portfolios the contribution of offshore wind along the entire coastline of China and onshore wind in east Inner-Mongolia remains nearly constant, meaning these assets may have the best return-volatility performance.

The case of wind & solar with constrained technology shares (40% wind +60% solar) clearly shows differing patterns of spatial distribution from wind & solar (see Fig. 15). Onshore wind assets are initially sporadically dispersed in east Inner-Mongolia, Northeast, Northwest and North China in the minvol portfolio, but they become increasingly concentrated in east Inner-Mongolia as the portfolio return increases (minvol versus minCV and maxret). Meanwhile, the coverage of offshore wind assets reduces gradually on the northern Chinese coastline.

Table 8
Potential-weighted average CF for each technology.
Source: Based on authors' analysis.

Technology		Potential-weighted average CF	Min mean CF of individual asset	Max mean CF of individual asset
Onshore wind	High	0.351	0.241	0.535
	Medium	0.347		
	Low	0.354		
Offshore wind	High	0.340	0.235	0.537
	Medium	0.340		
	Low	0.340		
Solar		0.208	0.158	0.278
Of which	Utility-PV	0.209		
	Rooftop PV	0.184		

[12] For comparison, the average electricity consumption of China in 2018 is 6840 TWh [80].

[13] Note not all VRE assets are included in optimal portfolios positioned on the efficient frontier. The selection of certain VRE assets in optimal portfolios is a result of the optimization. In general, for the same portfolio type, more assets are included in efficient frontiers facing a higher capacity budget.

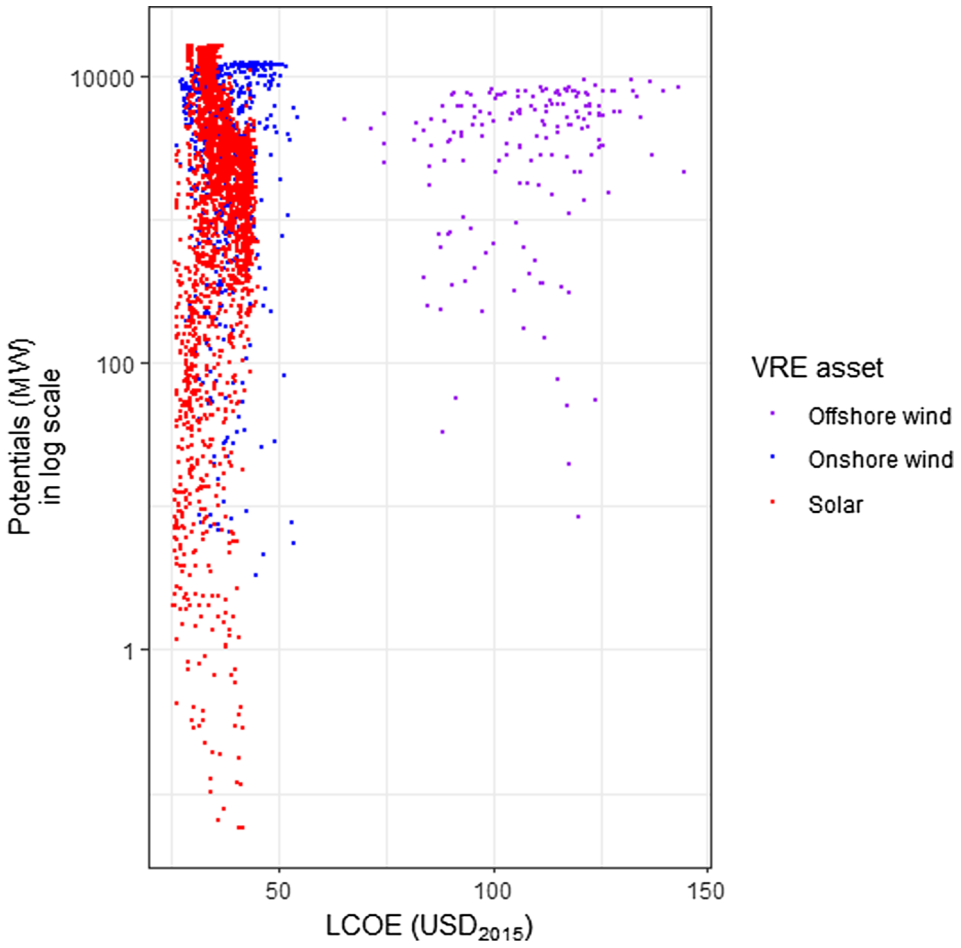

Fig. 11. Scatter plot of LCOE against potentials (in log scale) for each VRE asset (in medium case).
Source: Based on authors' analysis.

This leaves onshore and offshore wind assets with the highest mean CF in the maxret portfolio. As for solar assets, their contributing weights in the Northeast and the west of Northwest China increase from the minvol portfolio to the minCV portfolio, at the expense of decreased contributing weights in Southeast China. However, solar assets in these areas disappear in the maxret portfolio. Instead, they have a fairly large coverage in Inner-Mongolia, Southeast and the east of Northeast China.

The different spatial distributions of VRE assets explain the relatively better return-volatility performance of wind & solar portfolios with unconstrained technology shares compared with wind & solar portfolios with constrained technology shares. The latter has a greater degree of freedom to select the best VRE assets. Therefore, scenarios with predefined technology shares in existing literature might be sub-optimal in terms of return-volatility performance.

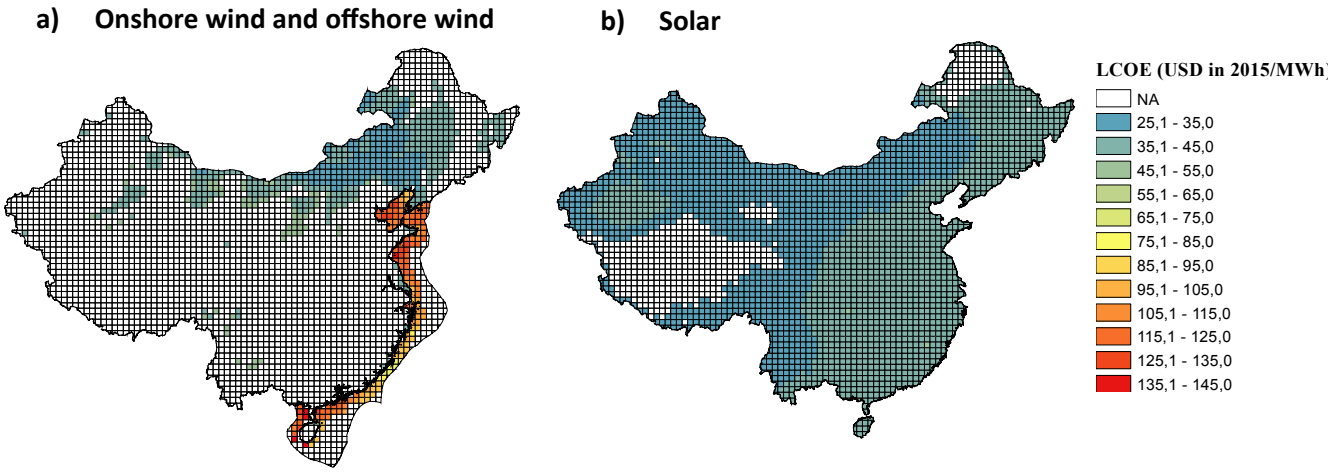

Fig. 12. Spatial distribution of LCOE per VRE asset in China (in medium case).
Source: Based on authors' analysis.

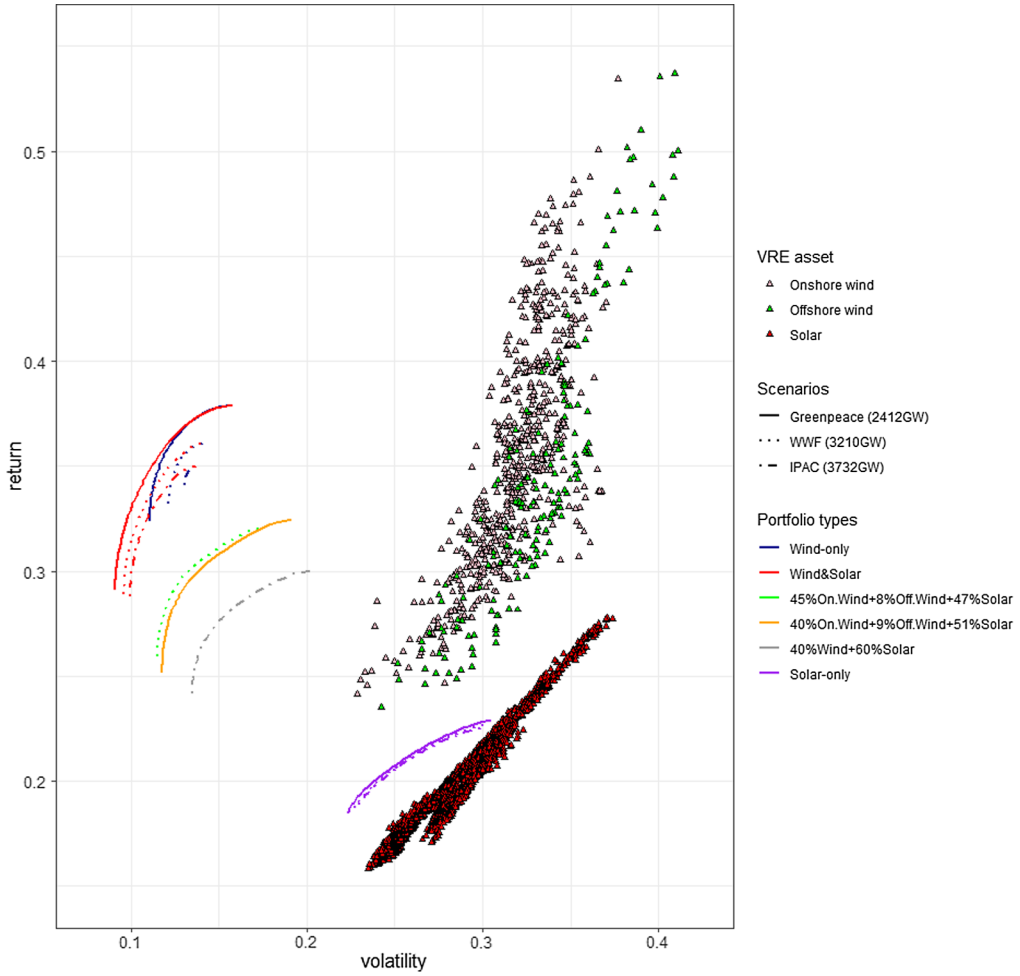

Fig. 13. Efficient frontier for portfolios with unconstrained and constrained technology shares.
Source: Based on authors' analysis.

3.7. Portfolio share per VRE technology

Fig. 16 illustrates the share of each VRE technology against the portfolio return for the wind & solar portfolio within the three different scenarios. Two key results are observed. Firstly, within all scenarios, solar is gradually replaced by onshore wind from the minvol portfolio (leftmost point) to the maxret portfolio (rightmost point), as the portfolio return increases[14] (and with it the portfolio volatility). Onshore wind (with a share above 50%) dominates all portfolios, but it faces a ceiling at 82%, even in the maxret scenario. The maximum solar share (23–28%) is observed in the minvol portfolio, and it decreases to close-to-zero in the maxret portfolio. This again confirms the relatively sub-optimal return-volatility performance of wind & solar portfolios with constrained technology shares (see Fig. 13). Secondly, the share of offshore wind is almost constant at 20% (± 2%), except for the Greenpeace scenario having the lowest capacity budget. This may suggest a low correlation between the power output of offshore wind and other VRE technologies. The share of offshore wind within the Greenpeace scenario decreases from initially ~25% in the minvol portfolio, to ~20% in the maxret portfolio. Since the low capacity budget of the scenario (2412 GW) is easy to meet, offshore wind is replaced by extra onshore wind assets with better mean CF.

3.8. Portfolio LCOE

We present the portfolio LCOE against the portfolio volatility[15] for multiple portfolio types within different scenarios in Fig. 17. On the one hand, within the same scenario, portfolio types with higher solar share (solar-only, wind &solar with constrained technology shares versus wind & solar, wind-only) tends to show lower portfolio LCOE, because of low LCOE of solar assets. On the other hand, the portfolio LCOE generally decreases with increased portfolio volatility (and thus increased portfolio return) along the efficient frontier. Highest and lowest portfolio LCOE are respectively observed in the minvol (most left point) and maxret (most right point) portfolio. This might seem counter-intuitive, as the portfolio share of solar (with low LCOE) decreases along the efficient frontier. The explanation is that low-CF assets are replaced by high-CF assets at the same time, dominating the overall decreasing trend of LCOE. In addition, it should be stressed that LCOE only covers the *production* costs of VRE, which exclude the integration costs of VRE imposed on the power system [7].

[14] To avoid misinterpretation, the authors stress that a portfolio with higher return is by no means better than a portfolio with lower return positioned on the same efficient frontier because the higher return portfolio also entails higher volatility. Both portfolios are efficient in terms of the return-volatility trade-off.

[15] The reason to plot the portfolio LCOE against the portfolio volatility (instead of portfolio return) is for the best visualization. If we plot the portfolio LCOE against the portfolio return, the curves seem to stack together. The key message of the graph does not depend on choosing volatility or return as the x-axis value, since the same trend is followed.

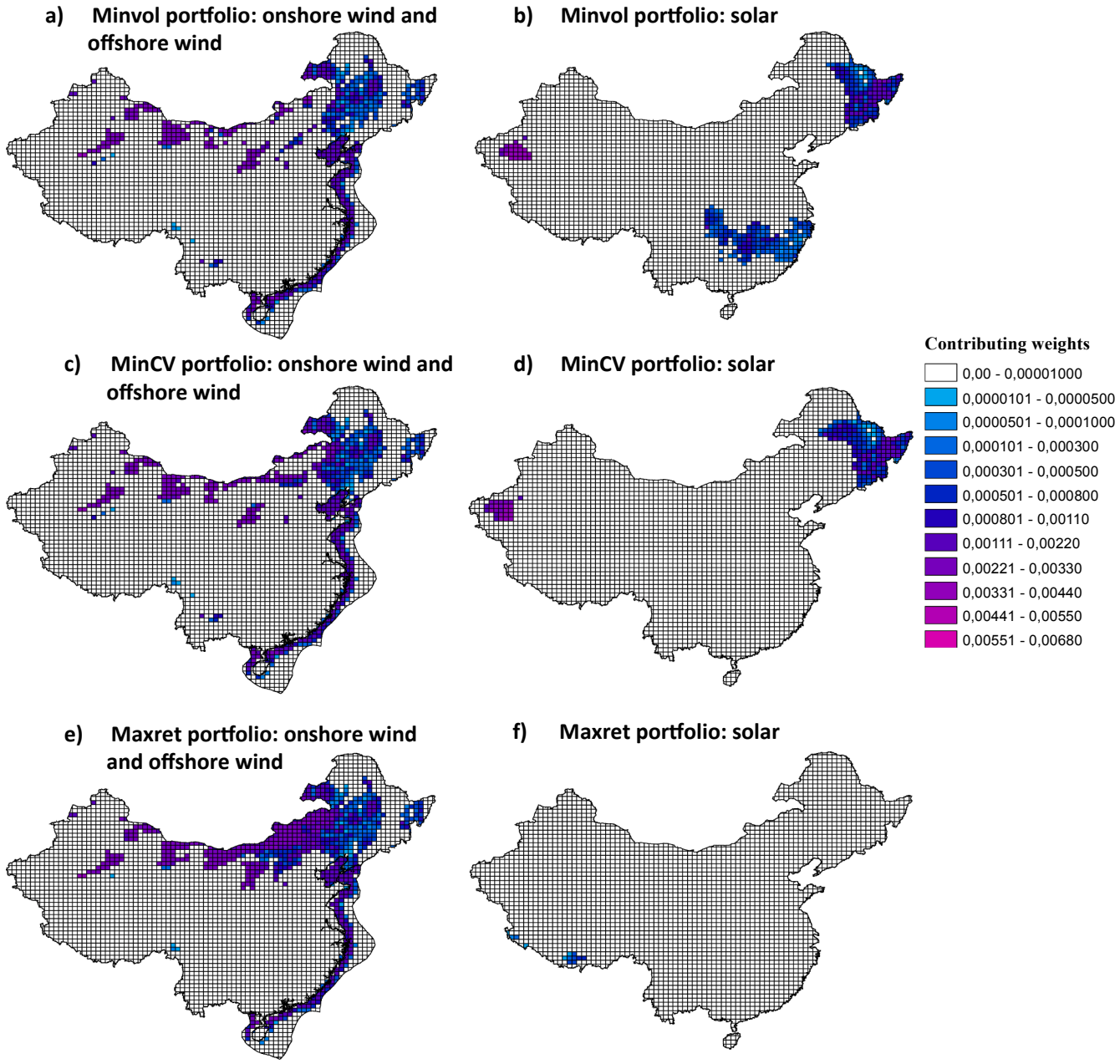

Fig. 14. Spatial distribution of contributing weights for the minvol, minCV and maxret wind & solar portfolios.
Source: Based on authors' analysis.

3.9. Portfolio CF duration curve and CF-at-risk

Using the IPAC scenario as an example, Fig. 18 presents the long-time portfolio CF duration curve based on the 16-year CF time series for the minvol, minCV and maxret portfolios positioned on the efficient frontier of wind & solar and wind & solar with constrained technology shares. Note that the portfolio return is represented by the area underneath the duration curve. For either wind & solar or wind & solar with constrained shares, the areas underneath the curve is largest for the maxret portfolio and lowest for the minret portfolio. By contrast, the overall steepness of CF duration curve (in terms of the slope of the linear fit of the curve) is lowest for the minvol portolio, then the minCV portfolio and maxret portfolio. Therefore, the minvol portfolio may be preferable to support power system operation due to its most stable power output. In addition, the CF duration curve of portfolios positioned on the wind & solar frontier with unconstrained technology shares tends to be less steep than the same portfolio positioned on the frontier of wind & solar with constrained technology shares. This implies that scenarios with pre-defined shares of various VRE technologies might be sub-optimal for supporting system operation.

The long-time CF-at-risk values can be obtained from the CF duration curve. For instance, here the $CF_{100\%}$ (available time 1.00) for the minvol, minCV and maxret wind & solar portfolios are respectively 0.049, 0.052 and 0. 044. This suggests that the portfolios with the highest CF-at-risk values are not necessarily the minvol portfolio, i.e. the tail risk should not be confused with volatility [68].

To better understand the behaviour of the long-time $CF_{100\%}$ and $CF_{90\%}$ along the efficiency frontier of multiple portfolio types within the three different scenarios, Fig. 19 was constructed. Note that the solar-only portfolio type is excluded because its $CF_{100\%}$ and $CF_{90\%}$ are zero due to the diurnal pattern of solar power output. It clearly shows that, in case portfolio return increases from the minvol to the maxret

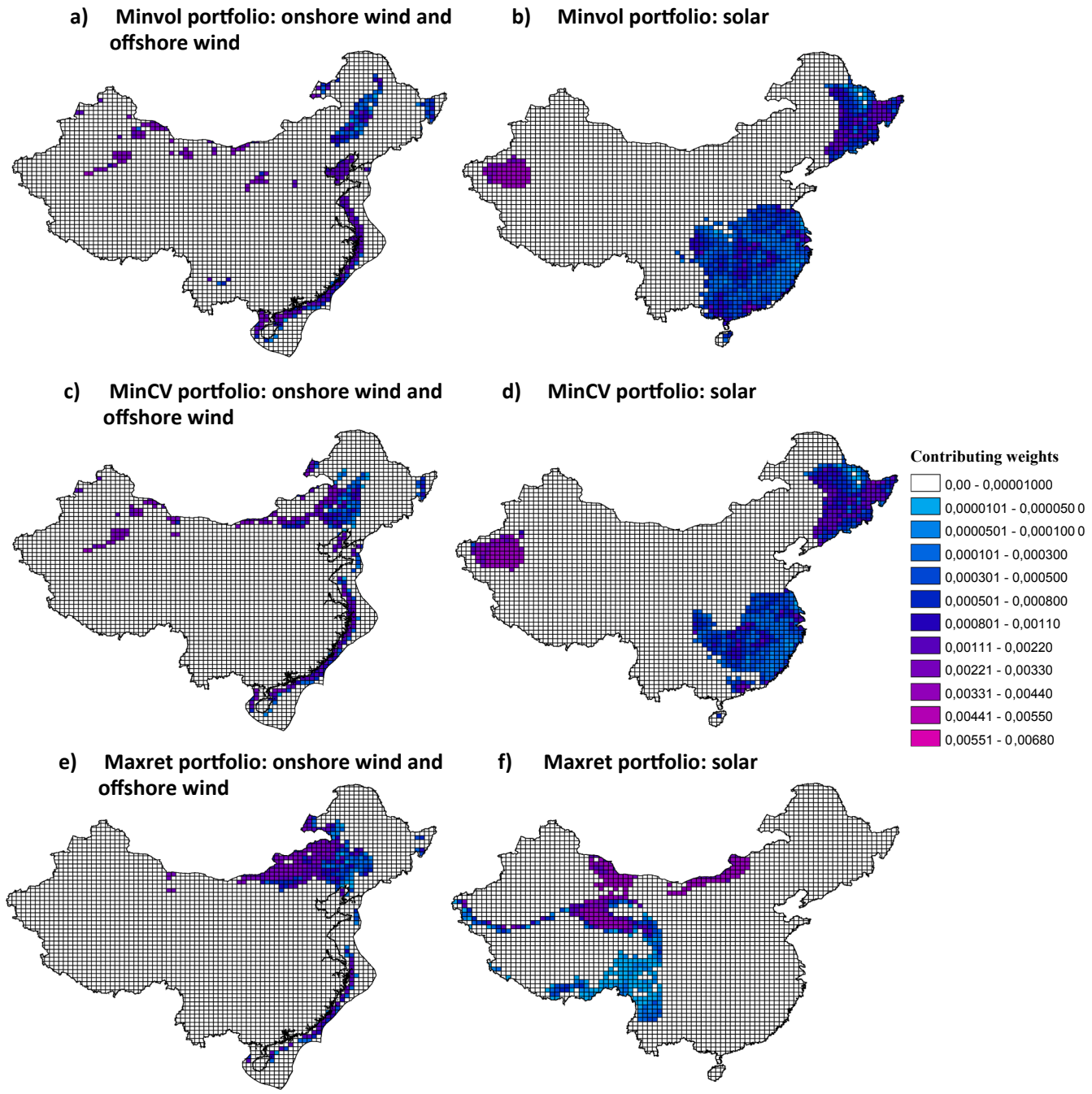

Fig. 15. Spatial distribution of contributing weights for the minvol, minCV and maxret wind & solar portfolios with constrained technology shares.
Source: Based on authors' analysis.

portfolio, the $CF_{90\%}$ first increases to a maximum value[16] and then decreases. It seems a similar tendency also exists for the $CF_{100\%}$, but it is less distinguishable due to the presence of noises. A possible explanation for these might be that it is difficult for the $CF_{100\%}$ to exhibit statistical significance as it is the most extreme value of the long-time time series of portfolio CF. We also observe that within the same scenario, both $CF_{90\%}$ and $CF_{100\%}$ are highest for the wind & solar portfolios with unconstrained technology shares, then for wind-only portfolios and lowest for the wind & solar portfolios with constrained technology shares. This reflects the benefit of diversification under the lowest constraints.

Next to the long-time $CF_{100\%}$ and $CF_{90\%}$, we also analysed the distribution of annual $CF_{100\%}$ and $CF_{90\%}$ obtained from the annual CF duration curve to investigate the inter-annual variation. Using the portfolio type of wind & solar and wind & solar with constrained technology shares within the IPAC scenario as an example, we present the distribution of annual $CF_{100\%}$ and $CF_{90\%}$ for five selected portfolios (minvol, minCV, maxret, $maxCF_{100\%}$ and $maxCF_{90\%}$) positioned on the efficient frontier in Fig. 20. To serve as a benchmark, the long-time values of $CF_{100\%}$ and $CF_{90\%}$ (indicated by the red point) are also shown. The spread and thickness of the distribution curve respectively represent the inter-annual variation and probability density of the sampled annual $CF_{100\%}$ and $CF_{90\%}$. We find that, firstly, the distribution of

[16] Note the portfolios associated with the maximum $CF_{100\%}$ and $CF_{90\%}$ along the efficient frontier are respective the $maxCF_{100\%}$ portfolio and $maxCF_{90\%}$ portfolio.

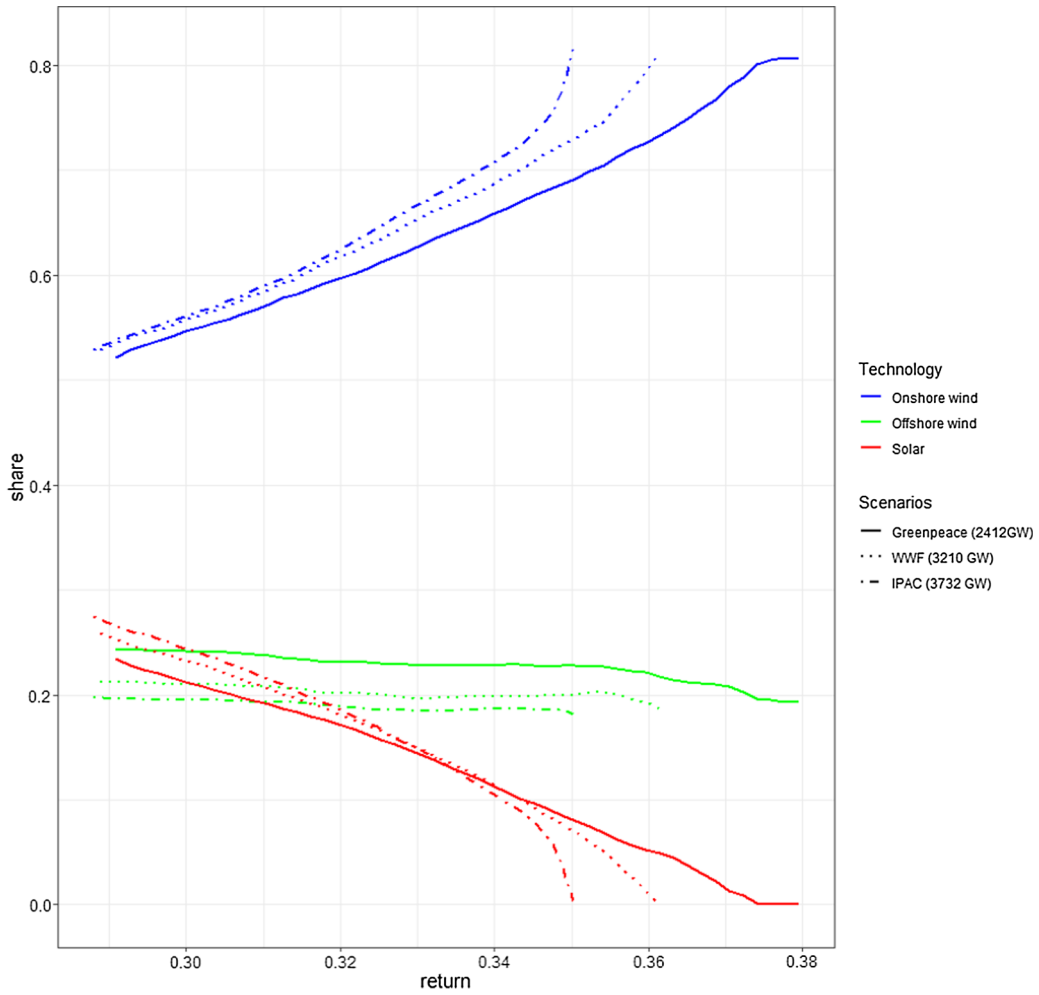

Fig. 16. Portfolio share per VRE technology for wind & solar portfolios within different scenarios. Source: Based on authors' analysis.

$CF_{100\%}$ is nearly symmetrical, and the long-time $CF_{100\%}$ is the lowest value of the annual $CF_{100\%}$. By contrast, the $CF_{90\%}$ is negatively skewed (and therefore has more downside tail risks), and the long-time $CF_{90\%}$ nearly coincides with the median $CF_{90\%}$. Secondly, the portfolio $CF_{100\%}$ is rather small and never exceeds 10%, whereas the portfolio $CF_{90\%}$ is 2–3 times the size of $CF_{100\%}$. Since 90% is the availability of coal-fired plants, the $CF_{90\%}$ can be grossly interpreted as the percentage of the capacity of coal that can be replaced by the VRE portfolio. However, the long spread of the sample distribution also suggests that the inter-annual variation of $CF_{100\%}$ and $CF_{90\%}$ can be large, and hence cannot be ignored. Therefore, caution should be given when using the long-time and annual $CF_{100\%}$ and $CF_{90\%}$ to support the operation of a future power system[17]. In addition, we also observe that the distribution spread of $CF_{100\%}$ and $CF_{90\%}$ for wind & solar with unconstrained technology shares is higher than that for wind & solar with constrained technology shares. This might be explained by the smaller inter-annual variation of solar power output (having higher shares in the constrained portfolios) in comparison with wind.

4. Discussion

Due to the scope, assumptions and data inputs of this study, a few limitations and uncertainties exist.

- The scope of this paper is limited to the geographical smoothing effect of portfolio volatility for each possible return level. We do not explicitly consider the geographical smoothing of portfolio output ramps and portfolio output forecast errors, which can also be investigated through MPT. This means that the optimum portfolios identified here may be different when these factors are considered, and more specifically the balance between wind and solar assets. However, we expect the difference to be small because of the benefits of diversification.
- Hourly meteorological reanalysis data was used to simulate the hourly VRE power output (in form of CF) and determine the efficient frontier of the return-volatility trade-off. This can mask the sub-hourly volatility of VRE. Shahriari and Blumsack [23] show that for the same portfolio return, the volatility over a ten-minute scale is larger than that over an hourly scale. In this sense, sub-hourly data captures the output profile of VRE more precisely and closer-to-real-time. This is important for the management of operating reserves, demand response, storage and other flexible resources, but is beyond the scope of this paper.
- This study is based on the assumption of a copperplate, due to the lack of high-resolution data of the transmission grid in China. Therefore, the optimal VRE portfolios obtained in this study may not be achievable considering the current transmission grid in China. However, our results help identify grid bottlenecks and plan grid expansion in China to harvest the benefits associated with

[17] Nevertheless, if the data sample is large enough, the extreme value theory can be used to fit the sample distribution to a generalized extreme value distribution. This can be used to forecast the probability associated with more extreme future CF-at-risk values.

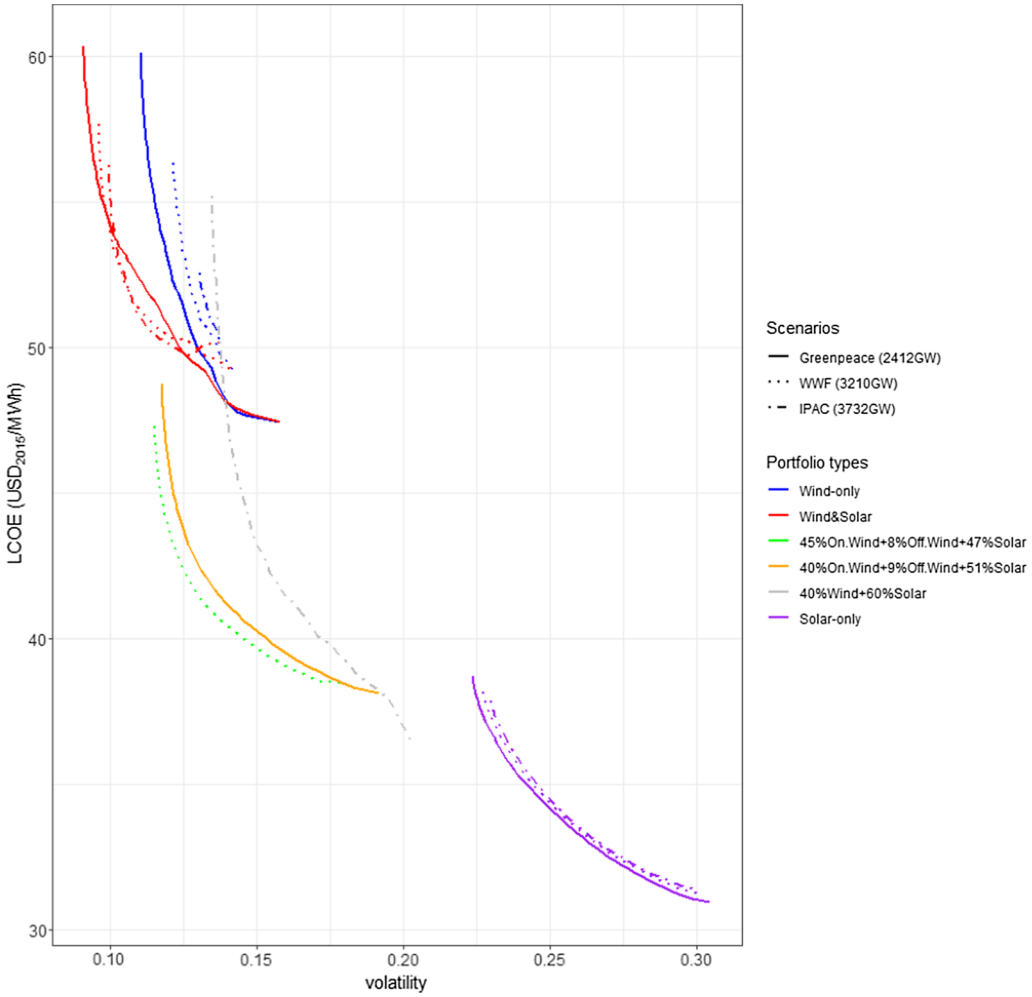

Fig. 17. Portfolio LCOE for multiple portfolio types within different scenarios.
Source: Based on authors' analysis.

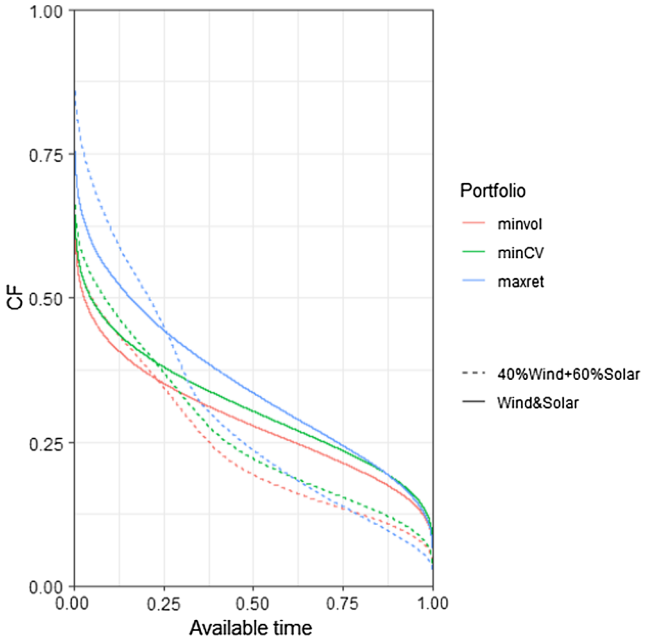

Fig. 18. Long-time portfolio CF duration curve for Wind & Solar and Wind & Solar with constrained technology shares within the IPAC scenario.
Source: Based on authors' analysis.

geographical smoothing in the most optimal way. Once grid-related data is available, it can be treated as additional constraints in the MPT optimization [26] or incorporated into the optimization objective function [31]. Transmission constraints shift the efficient frontier rightwards, resulting in less optimal portfolios than portfolios without transmission constraints [31]. The accuracy of incorporating transmission constraints can be improved by the support of a detailed power flow model based on Kirchhoff's laws [82].

- While the purpose of developing optimal VRE portfolios is to better serve the balance between electricity supply and demand, this paper does not explicitly consider the (hourly) demand profile for China. Besides the lack of reliable data at national and regional levels, the demand profile in the long-term future (e.g. 2050) depends on the highly uncertain trend of electrification and the structural change of the economy. In addition, considering the increasing popularization of smart-grid technology and real-time pricing that encourage demand response, the demand profile can become more flexible and adaptable to VRE outputs. We propose scenario-based studies in future research to explore these areas. Once robust data on the demand profile is available, it can be fed into the MPT optimization. For instance, the sum of regional demand and total export transmission capacity can be set as a ceiling for the regional maximum installed VRE capacity [26]. Alternatively, the portfolio return and volatility can be formulated as the mean and standard deviation of the residual demand (demand less VRE output) respectively, which helps to increase the match between VRE output and demand [21].

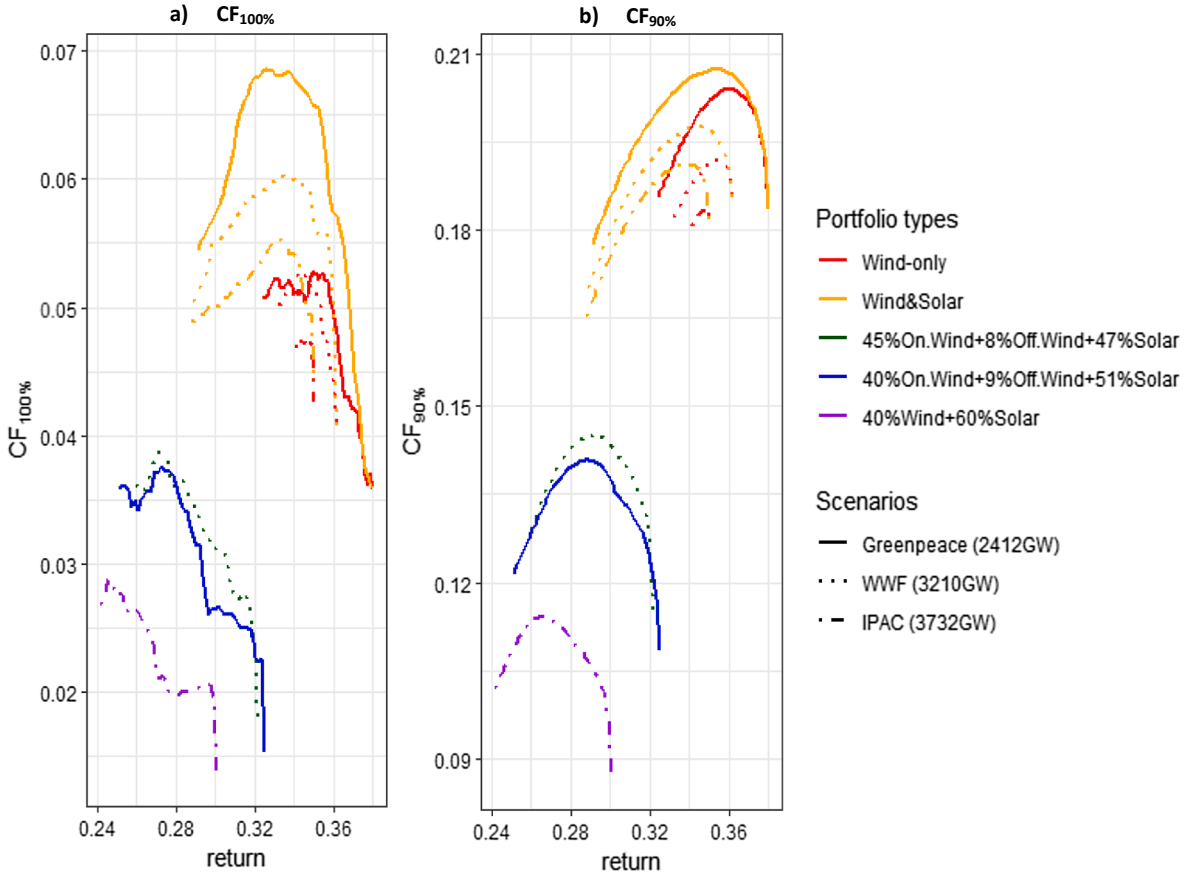

Fig. 19. $CF_{100\%}$ and $CF_{90\%}$ of multiple portfolio types within different scenarios.
Source: Based on authors' analysis.

- Regarding the determination of hourly CF time series for wind and solar, a few simple assumptions have been made in the absence of detailed models. For instance, we did not explicitly consider the wake effect (although the selected intermediate spacing implicitly avoids large wake losses) and the smoothing effect resulting from wind speed propagation within a wind farm. This can lead to an overestimation of the mean and volatility of wind's capacity factor. For solar, we assumed a uniform PR at 85% for all solar installations in China. The PR is dependent on the efficiency of the PV system and the module temperature [83]. Although not corrected for the inter-regional differences in weather conditions (solar irradiance, wind speed and ambient temperature) that affect the module temperature, the PR at 85% on average is a realistic assumption for the long-term future (see footnote 7). In addition, we determined optimal angles for both utility-PV and rooftop PV to maximize the total yields per installation, assuming they are both mounted on a surface close to flat. These angles can increase the portfolio return, but are not necessarily preferable to minimize the portfolio volatility. We propose future studies to investigate alternative PV angles and their impact on the efficient frontier.
- We used geographical potentials per VRE asset as constraints (maximum installed capacity per asset) in the MPT optimization. These potentials were estimated based on multiple geographical and social acceptance constraints and land cover suitability factors from literature. Although validating these constraints and suitability factors is beyond the scope of this study, their uncertainties can cause increased or decreased potentials. For instance, the threshold distance to (dense) urban area and shore for onshore and offshore were conservatively set at 10 km. Alternative threshold distances may lead to different potentials and affect the spatial distribution of optimal portfolios.
- To analyse the economics of optimal VRE portfolios, we determined the portfolio LCOE. However, LCOE is an incomplete indicator, as it only covers the unit production cost and does not capture the system-wide costs resulting from adding VRE into the power system. On the one hand, optimal VRE portfolios positioned on the efficient frontier may displace more capacity and production from conventional fossil-fired power plants and minimize the impact of variability on the power system, leading to system cost reduction. On the other hand, additional investment in transmission infrastructure may be required to connect VRE assets with each other and with the electricity consumers. Costs and savings associated with these system-wide impacts are best assessed by more comprehensive indicators such as levelized avoided cost of electricity [84], system LCOE [7] and value-adjusted LCOE [85]. This, however, necessitates the development of baseline and reference scenarios based on power system modelling, which can be covered in future research.
- This study identified optimal VRE portfolios in terms of the spatial distribution of different VRE assets based on a greenfield situation, without considering existing VRE capacity in China. This is helpful to explore the theoretically maximum geographical smoothing effect. Nevertheless, such greenfield situation is difficult to meet, given the sunk nature of VRE investments in reality. Alternatively, existing VRE capacity can be framed as constraints in the MPT optimization in future studies. This is expected to reduce the "efficiency" of optimal portfolios in terms of the return-volatility performance. Moreover, optimal portfolios are best achieved through a social planner that makes centralized investment decisions. However, in reality investment decisions for each VRE installation are made by individual investors through project financing or corporate financing. These investors may not be attracted by individual sub-optimal installations, even if they are indispensable to optimize

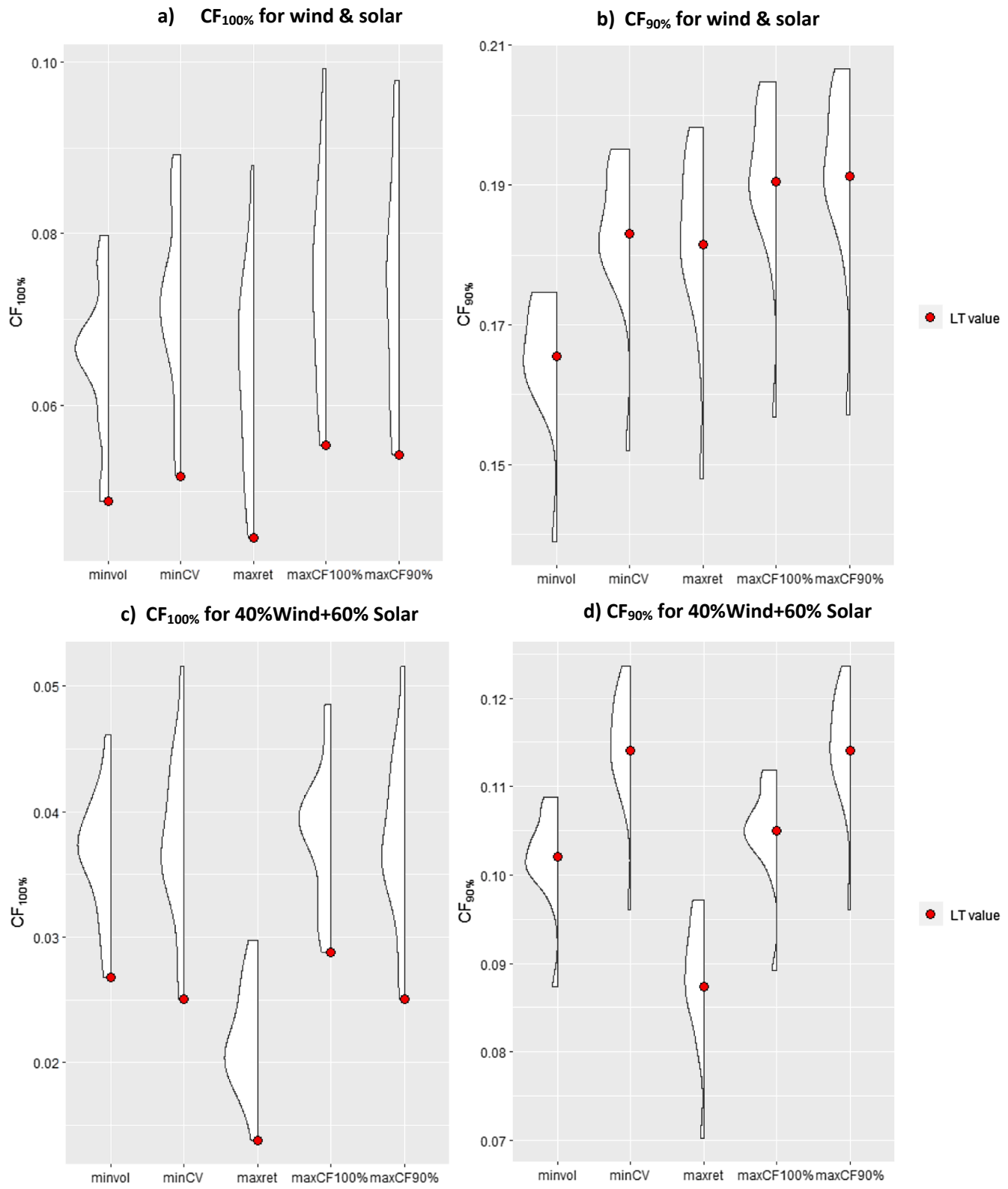

Fig. 20. Distribution of annual $CF_{100\%}$ and $CF_{90\%}$ for wind & solar and wind & solar with constrained technology shares within the IPAC scenario. Source: Based on authors' analysis.

the overall portfolio. Therefore, effective and pragmatic development pathways are essential to achieve optimal portfolios, which require smart policy measures and market designs to steer VRE investments. However, this is beyond the scope of the present work. Roadmap studies are recommended to further analyse this issue.

- We determined the long-time $CF_{100\%}$ and $CF_{90\%}$ for selected optimal portfolios. They are 100- and 90-percentile values of the 16-year hourly portfolio CF time series, and hence they represent the minimum portfolio CF that is available 100% and 90% of time. As a common practice in MPT literature within the field of economics

and finance, the at-risk-value derived from a long-time time series of the underlying variable (e.g. portfolio financial return) is often interpreted as a time-invariant minimum value associated with a given probability [86]. Based on the *ergodicity hypothesis* originated from statistic mechanics, over a long-time period (close-to-infinity), the distribution of a stochastic process across time approaches its distribution across ensembles (i.e. all possible stochastic realizations) [86]. In this sense, it seems plausible to interpret $CF_{100\%}$ and $CF_{90\%}$ as the minimum CF associated with 100% and 90% probability. While the ergodicity hypothesis (if true) helps to reduce uncertainties associated with unobservable ensemble distribution, it is virtually impossible to prove [87]. Being a strong assumption, its wide usage in economics and finance also leads to many criticisms [88,89]. Therefore, $CF_{100\%}$ and $CF_{90\%}$ should never be misinterpreted as the minimum CF associated with 100% and 90% probability. Rather, they represent the minimum portfolio CF with 100% and 90% availability.

- Based on key statistics (mean, standard deviation and covariance matrix) derived from historical meteorological reanalysis data, we used MPT to obtain optimal VRE portfolios for China in the (long-term) future. This can give rise to two main limitations. Firstly, despite its general accessibility and global coverage, reanalysis data entails model uncertainties. For instance, they often erroneously predict actual clear-sky conditions as cloudy and lack detailed representation of local terrain conditions [37,90]. This can result in biased estimates of key statistics derived from reanalysis data. This bias, however, can be corrected through validation and calibration with historically observed VRE output data [91]. Further research on this is recommended, once observed real data for China becomes more accessible. Secondly, drawing conclusive statistics for and between different VRE assets typically requires a long-time period of 15–30 year [92]. Although we used a 16-year historical period of weather data, its key statistics may not well represent the long-term future (e.g. due to non-stationarity). This is further complicated by the uncertain impact of climate change on future weather, which is not considered in this study. We propose studies based on climate modelling to investigate this issue specifically for China.

5. Conclusion

In this study, we optimized portfolios of VRE assets using MPT to capture the geographical smoothing effect in China's future power system. The geographical smoothing effect in terms of better return-volatility performance of VRE outputs is expected to bring about multiple benefits to support power system operation. Based on the copperplate assumption, efficient frontiers of optimal VRE portfolios were determined for different scenarios and portfolio types. We also characterized key portfolio statistics (spatial distribution, technology shares, LCOE, CF-at-risk) to understand their behaviour along the efficient frontier.

Main findings of this study are:

- This study shows that China has vast geographical potentials for VRE. The maximum capacity that can be installed is 575–4909 GW for onshore wind, 559–932 GW for offshore wind and 12,936 GW for solar. The geographical potentials and mean CF determined at each VRE asset level also provide necessary information for policy-makers, academic peers and private investors to evaluate the performance of VRE resources. For instance, they can be used to guide decision-making in project financing of VRE investment. They also support the design of efficient subsidy schemes necessary to reach China's renewable energy targets. The best resources (in terms of both high mean CF and high potentials) are found in Inner-Mongolia (for wind) and North China (for solar).
- Optimal portfolios positioned on the efficient frontier exhibit superior return-volatility performance compared to individual VRE assets in China. The geographical distribution of VRE assets in optimal portfolios provides a rationale for the allocation of national renewable energy targets to different provinces in China. It can help policy-makers to plan and coordinate the development of different VRE assets as well as the transmission grid in a more system-optimized manner. This is expected to bring about significant economic benefits in power system investment and operation. Within the same efficient frontier, portfolios with a higher return also entail a higher volatility. It must be stressed that these portfolios are all efficient, as the portfolio risk is minimized for each attainable return level. Therefore, the selection of portfolios within the efficient frontier is purely a policy decision, depending on the prevailing return-volatility preference.
- The efficient frontier of wind & solar portfolios exhibits better return-risk performance than wind-only and solar-only frontiers. This suggests complementarity between wind and solar in China. Strong negative correlations in power output exist between wind assets in east Inner-Mongolia, Northeast, Northwest and North China and solar assets in Northeast, Northwest and East China. Therefore, it is advisable for policy-makers to coordinate the investment and development of VRE assets in these regions to capture the benefits of diversification. We also demonstrated that for the same total installed capacity, wind & solar portfolios with unconstrained technology shares exhibit better return-volatility performance than portfolios with constrained technology shares. This suggests that existing scenarios in literature with pre-defined shares of different VRE technologies might be sub-optimal to support power system operation. Hence, it is crucial for these scenarios to be thoroughly assessed and reviewed before they are used in policy decision-making.
- With increased portfolio volatility (and portfolio return), the LCOE of wind & solar portfolios decreases along the efficient frontier. Although the portfolio share of solar (with low LCOE) decreases along the efficient frontier, low-CF assets are meanwhile replaced by high-CF assets. The latter factor dominates the overall decreasing trend of LCOE.
- VRE technologies in literature and mass media are often portrayed as "intermittent renewable energy sources". The lexical definition of "intermittency" suggests an on-and-off pattern in VRE outputs. This can lead to a biased impression of VRE technologies, i.e. that they are unreliable. While "intermittency" fairly characterizes the output pattern per VRE installation, the collective VRE output pattern is more important from the perspective of power system operation. We argue that "intermittency" should not be used to characterize the collective output pattern of well-diversified VRE assets spread over a large geographical area. This is supported by the results of this study. The long-time $CF_{100\%}$ for wind & solar portfolios suggests that a non-zero minimum portfolio CF (1.4–5.5%) can exist with 100% availability.

Acknowledgement

This work is part of the research programme "Transitioning to a More Sustainable Energy System" with project number 022.004.023, which is financed by the Netherlands Organisation for Scientific Research (NWO). The authors would like to thank Dennis Swanink and Remco de Boer for support of extracting reanalysis data, Ivan Vera and Maarten Zeylmans van Emmichoven for technical support of ArcGIS, Vasileios Daioglou for support of R programming, Atse Louwen for debugging PV-related calculations, Madeleine Gibescu for inspiring discussions and recommendations, and Kay McLeod for the proof-reading. Two anonymous reviewers are also thanked for improving the clarity and quality of this paper.

References

[1] IEA. World Energy Outlook 2015. Paris: International Energy Agency (IEA); 2015.
[2] Crijns-Graus W. Renewable energy: past trends and future growth in 2 degrees scenarios. 3rd International Conference on Power and Energy Systems Engineering CPESE 2016, 8-12 September 2016, Kitakyushu, Japan, Energy Procedia 2016;vol. 100(2016):14–21.
[3] REN21 (2018), Renewables 2018 Global Status Report, Renewable Energy Policy Networks for the 21st.
[4] Samadi S. The experience curve theory and its application in the field of electricity generation technologies – A literature review. Renew Sustain Energy Rev 2018;82(2018):2346–64.
[5] Portugal-Pereira J, Esteban M. Implications of paradigm shift in Japan's electricity security of supply: A multi-dimensional indicator assessment. Appl Energy 2014;123(2014):424–34.
[6] Banks JP, Boersma T, Goldthorpe W. Challenges related to carbon transportation and storage showstoppers for CCS? The Global CCS Institute; 2017.
[7] Ueckerdt F, Hirth L, Luderer G, Edenhofer O. System LCOE: what are the costs of variable renewables? Energy 2013;63(2013):61–75.
[8] Luickx PJ, Delarue ED, D'haeseleer WD. Considerations on the backup of wind power: Operational backup. Appl Energy 2008;85(2008):787–99.
[9] Ela E, Milligan M, Kirby B. Operating Reserves and Variable Generation: A comprehensive review of current strategies, studies, and fundamental research on the impact that increased penetration of variable renewable generation has on power system operating reserves. Natl Renew Energy Laboratory (NREL) 2011. 2011.
[10] Gonzalez-Aparicio I, Zucker A. Impact of wind power uncertainty forecasting on the market integrationof wind energy in Spain. Appl Energy 2015;159(2015):334–49.
[11] IEA. The power of transformation: Wind, Sun and the Economics of flexible power systems. Paris: International Energy Agency (IEA); 2014.
[12] Monforti F, Huld T, Bodis K, Vitali L, D'Isidoro M, Lacal-Arantegui R. Renew Energy 2014;63(2014):576–86.
[13] Fertig E, Apt J, Jaramillo P, Katzenstein W. The effect of long-distance interconnection on wind power variability. Environ Res Lett 2012;77.
[14] Girard R, Laquaine K, Kariniotakis G. Assessment of wind power predictability as a decision factor in the investment phase of wind farms. Appl Energy 2013;101(2013):609–17.
[15] Kiviluoma J, Holttinen H, Weir D, Scharff R, Soder L, Menemenlis N, Cutululis NA, Lopez ID, Lannoye E, Estanqueiro A, Gomez-Lazaro E, Zhang Q, Bai J, Wan Y-H, Milliagn M. Variability in large-scale wind power generation. Wind Energy 2016;19(2016):1645–65.
[16] Muzhikyan A, Farid AM. Mezher T. The impact of wind power geographical smoothing on operating reserve requirements. In: 2016 America Control Conference (ACC), Boston Marriott Copley Place, July 6-8th, 2016; 2016.
[17] Pinson P. Estimation of the uncertainty in wind power forecasting, PhD-thesis, Engineering Sciences [physics], École Nationale Supérieure des Mines de Paris, 2006; 2006.
[18] Elton EJ, Gruber MJ, Goetzmann WN, Brown SJ. Modern portfolio theory and investment analysis. 9th ed. New York: John Wiley & Sons; 2013.
[19] Koivisto MJ, Cutululis NA, Ekstrom J. Minimizing variance in variable renewable energy generation in Northern Europe. In: 2018 IEEE International Conference on Probabilistic Methods Applied to Power Systems, Boise, United States; 2018.
[20] Drake B, Hubacek K. What to expect from a greater geographic dispersion of wind farms?—A risk portfolio approach. Energy Policy 2007;35(2007):3999–4008.
[21] Degeilh Y, Singh C. A quantitative approach to wind farm diversification and reliability. Electr Power and Energy Syst 2011;33:303–13.
[22] Tejeda C, Gallardo C, Dominguez M, Gaertner MA, Gutierrez C, de Castro M. Using wind velocity estimated from a reanalysis to minimize the variability of aggregated wind farm production over Europe. Wind Energy 2018;21-3:174–83.
[23] Shahriari M, Blumsack S. The capacity value of optimal wind and solar portfolios. Energy 2018;148:992–1005.
[24] Srinivasan TN, Gopi Rethinaraj TS. Fukushima and thereafter: Reassessment of risks of nuclear power. Energy Policy 2013;52(2013):726–76.
[25] Perez-Moreno SS, Dykes K, Merz KO, Zaaijer MB. Multidisciplinary design analysis and optimisation of a reference offshore wind plant. J Phys: Conf Ser 2018;1037(2018):042004.
[26] Roques F, Hiroux C, Saguan M. Optimal wind power deployment in Europe—A portfolio approach. Energy Policy 2010;38:3245–56.
[27] Novacheck J, Johnson JX. Diversifying wind power in real power systems. Renew Energy 2017;106:177–85.
[28] Speth V. Diversification of Wind and Solar Energy Portfolio Risk: An Explorative Analysis for Germany 2010-2012, DISSERTATION of the University of St. Gallen, School of Management, Economics, Law, Social Science and International Affairs to obtain the title of Doctor of Philosophy in Management; 2013.
[29] Lima MAFB, Carvalho PCM, Carneiro TC, Leite JR, de Bessa Neto, Rodrigues GKL, de Melo FE. Portfolio theory applied to solar and wind resources forecast. IET Renew Power Gener 2017;11(7):973–8.
[30] Thomaidis NS, Santos-Alamillos FJ, Pozo-Vazquez D, Usaola-Garcia J. Optimal management of wind and solar resouces. Comp Oper Res 2016;66:284–91.
[31] Rombauts Y, Delarue E, D'haeseleer W. Optimal portfolio-theory-based allocation of wind power: taking into account cross-border transmission-capacity constraints. Renew Energy 2011;36(2011):2374–87.
[32] Santos-Alamillos FJ, Thomaidis NS, Usaola-Garcia J, Ruiz-Arias JA, Pozo-Vazquez D. Renew Energy 2017;106(2017):335–42.
[33] Huenteler J, Tang T, Chan G, Anadon LA. Why is China's wind power generation not living up to its potential? Environ Res Lett 2018;12(4).
[34] Liu and Chu. Wind power and photovoltaic power: How to improve the accommodation capability of renewable electricity generation in China? Int J Energy Res 2018;42–7(2018):2320–43.
[35] Jiang K, He C, Xu X, Jiang W, Xiang P, Li H, Liu J. Transition scenarios of power generation in China under global 2 °C and 1.5 °C targets. Global Energy Interconnection 2018;1(4):477–86.
[36] European Commission (2011), Communication from the Commission to the European Parliament, the Council, the European Economic and Social Committee and the Committee of the Regions, A Roadmap for moving to a competitive low carbon economy in 2050, Brussels, March 8th 2011.
[37] Sun Y-W, Hof A, Wang R, Liu J, Lin Y-J, Yang D-W. GIS-based approach for potential analysis of solar PV generation at the regional scale: A case study of Fujian Province. Energy Policy 2013;58:248–59.
[38] Herran DS, Dai H, Fujimori S, Masui T. Global assessment of onshore wind power resources considering the distance to urban areas. Energy Policy 2016;91(2016):75–86.
[39] Volker PJH, Hahmann AN, Badger J, Jorgensen HE. Prospects for generating electricity by large onshore and offshore wind farms. Environ Res Lett 2017;12(2017):034022.
[40] Global Administrative Areas (2012), GADM database of Global Administrative Areas, version 2.0, www.gadm.org, accessed on November 11th, 2018.
[41] Flanders Marine Institute (2018), Maritime Boundaries Geodatabase: Maritime Boundaries and Exclusive Economic Zones (200NM), version 10, http://www.marineregions.org/, accessed on Nov 11th, 2018.
[42] Eurek K, Sullivan P, Gleason M, Hettinger D, Heimller D, Lopez A. An improved global wind resource estimate for integrated assessment models. Energy Econ 2017;64(2017):552–67.
[43] British Oceanographical Data Centre (2015), Maritime Boundaries Geodatabase: Maritime Boundaries and Exclusive Economic Zones (200NM), version 10, http://www.marineregions.org/, [accessed on November 11th 2018].
[44] Peyrard C. Offshore wind turbine foundations, EDF R&D and Laboratoire d'Hydraulique St Venant (LNHE); 2015. https://formationemr16.sciencesconf.org/file/266745, [accessed on 27th Feb 2019].
[45] Halpern BS, Frazier M, Potapenko J, Casey KS, Koenig K, Longo C, et al. Cumulative human impacts: raw stressor data of 2013 commercial shipping activities, Knowledge Network for Biocomplexity (KNB); 2015. https://knb.ecoinformatics.org/view/doi:10.5063/F1S180FS, [accessed on November 11th 2019].
[46] Bosch J, Staffell I, Hawkes AD. Temporally explicit and spatially resolved global offshore wind energy potentials. Energy 2018;163(2018):766–81.
[47] Mahlknecht G. Greg's Cable Map Version 1.12; 2013. https://old.datahub.io/dataset/undersea-cables, [accessed on November 11th 2018].
[48] International Union for the Conservation of Nature and United Nations Environment Programme (2017), World Database on Protected Areas (WDPA), https://www.iucn.org/theme/protected-areas/our-work/quality-and-effectiveness/world-database-protected-areas-wdpa, accessed on November 11th, 2018.
[49] Gruber S. Derivation and analysis of a high-resolution estimate of global permafrost zonation. The Cryosphere (2012) 2012;6:221–33.
[50] United States Geological Survey (2018), Digital Elevation - Global 30 Arc-Second Elevation (GTOPO30), https://www.usgs.gov/centers/eros/science/usgs-eros-archive-digital-elevation-global-30-arc-second-elevation-gtopo30?qt-science_center_objects=0#qt-science_center_objects, [accessed on November 11th, 2018].
[51] Bontemps S, Van Bogaert E, Defourny P, Kalogirou V, Arino O. (2010), GlobCover 2009 – Products Description Manual, version 1.0, December 2010.
[52] Hoogwijk MM. On the global and regional potential of renewable energy sources PhD-thesis Science, Technology and Society, Utrecht University; 2004
[53] Deng YY, Haigh M, Rouwels W, Ramaekers L, Brandsma R, Schimschar S, et al. Quantifying a realistic, worldwide wind and solar electricity supply. Global Environ Change 2015;31(2015):239–52.
[54] IEC (2005), IEC 61400-1: Wind Turbine Generator (WTG) Classes.
[55] Wind-turbine-models.com (2015a), Vestas 117-3.3, https://en.wind-turbine-models.com/turbines/694-vestas-v117-3.3, accessed on November 11th, 2018.
[56] Wind-turbine-models.com (2015b), Vestas 126-3.3, https://en.wind-turbine-models.com/turbines/695-vestas-v126-3.3, accessed on November 11th, 2018.
[57] Wind-turbine-models.com (2015c), Vestas 164-8.0, https://en.wind-turbine-models.com/turbines/318-vestas-v164-8.0, [accessed on November 11th, 2018].
[58] WWF (2014), China's Future Generation Assessing the Maximum Potential for Renewable Power Sources in China to 2050, January 2014.
[59] De Jonge J, Hinz A, Oudes D, Luisman H. Zonneparken in het buitengebied van de provincie Flevoland: Een economische en ruimtelijke verkenning (Solar farms in the rural area of the Province of Flevoland), October 2017; 2017.
[60] Copper JK, Sproul AB, Bruce AG. A method to calculate array spacing and potential system size of photovoltaic arrays in the urban environment using vector analysis. Appl Energy 2016;161(2016):11–23.
[61] Staffell I, Green R. How does wind farm performance decline with age. Renew Energy 2014;66(2014):775–86.
[62] Zappa W, van den Broek M. Analysing the potential of integrating wind and solar power in Europe using spatial optimisation under various scenarios. Renew Sustain Energy Rev 2018;94(2018):1192–216.
[63] EWEA. Wind energy – the facts: a guide to the technology, economics and future of wind power. 1st ed. Oxford: Routledge; 2009. p. 2009.
[64] Wagner R, Antoniou I, Pedersen SM, Courtney MS, Jorgensen HE. The influence of the wind speed profile on wind turbine performance measures. Wind Energy 2009;12(2009):348–62.
[65] Libii JN. Comparing the calculated coefficients of performance of a class of wind turbines that produce power between 330 kW and 7,500 kW. World Trans Eng

Technol Edu 2013;11(2013):36–40.
[66] Svenningsen L. Proposal of an improved power curve correction. In: European Wind Energy Conference & Exhibition 2010, Warsaw, Poland (April 2010); 2010.
[67] Andrews J, Jelley N. Energy Science: principles, technologies and impacts. 3rd revised ed. Oxford, United Kingdom: Oxford University Press; 2017.
[68] Taleb NN. The Black Swan: the Impact of the Highly Improbable. 2nd ed. New York: Random House; 2010.
[69] Kalogirou SA. Solar Energy Engineering: Process and Systems. 2nd Edition Academic Press; 2016. 14th November 2013.
[70] Ridley B, Boland J, Lauret P. Modelling of diffuse solar fraction with multiple predictors. Renew Energy 2010;35(2010):478–83.
[71] Gulin M, Vasak M, Baotic M. Estimation of the global solar irradiance on tilted surfaces. 17th International Conference on Electrical Drives and Power Electronics (EDPE 2013). 2013.
[72] Litjens GBMA, Worrell E, van Sark WGJHM. Influence of demand patterns on the optimal orientation of photovoltaic systems. Sol Energy 2017;155(2017):1002–14.
[73] Reich NH, Mueller B, Armbruster A, van Sark WGJHM, Kiefer K, Reise C. Performance ratio revisited: is PR > 90% realistic? Progr Photovolt 2012;20(2012):717–26.
[74] IEA (2016), Power generation assumptions in the New Policies and 450 Scenarios in the World Energy Outlook 2016.
[75] Klinge Jacobsen H, Koch H, Alejandro P, Wolter C. Versus offshore: comparative cost and competitive advantages. IAEE Energy Forum (Bergen Special 2016) 2016:17–9.
[76] Lensink SM. Kosten IJmuiden-Ver in relatie tot Hollandse Kust, ECN-E–16-023, June 2016; 2016.
[77] Greenpeace, Global Wind Energy Council and SolarPower Europe (2015), energy [r]evolution: a sustainable world energy outlook 2015, 5th Report, September 2015.
[78] WWF (2015), China's Future Generation 2.0 Assessing the Maximum Potential for Renewable Power Sources in China to 2050, November 2015.
[79] Mills A, Wiser R. Implications of wide-area geographic diversity for short-term variability of solar power. Ernest Orlando Lawrence Berkeley National Laboratory, Environmental Energy Technologies Division; 2010. September 2010.
[80] China Electricity Council (2019), 2018 National Electric Power Industry Statistics Brief [in Chinese], http://www.cec.org.cn/d/file/guihuayutongji/tongjxinxi/niandushuju/2019-01-22/4fedb4c956f6059c5998913b10a6233a.pdf, [accessed on April 5th 2019].
[81] BNEF (2018), New Energy Outlook 2008, Bloomberg New Energy Finance.
[82] Erdener BC, Pambour KA, Lavin RB, Dengiz B. An integrated simulation model for analysing electricity and gas systems. Electrical Power Energy Syst 2014;61(2014):410–20.
[83] Dierauf T, Growitz A, Kurtz S, Cruz JLB, Riley E, Hansen C. Weather-Corrected Performance Ratio. National Renewable Energy Laboratory (NREL); 2013. Technical Report 2013.
[84] EIA. Levelized cost and levelized avoided cost of new generation resources in the annual energy outlook 2019. U.S. Energy Information Administration; 2019. p. 2019.
[85] IEA. World Energy Outlook 2018. Paris: International Energy Agency (IEA); 2018.
[86] Los CA. Financial market risk: measurement and analysis. Routledge International Studies in money and banking. London, UK: Taylor and Francis; 2003.
[87] Barkley Rosser J. Reconsidering ergodicity and fundamental uncertainty. J Post Keynesian Econ (2015) 2015;38–3:331–54.
[88] Davidson P. Is probability theory relevant for uncertainty? A post keynesian perspective. J Econ Perspect 1991;5–1:129–43.
[89] Peters O, Gell-Mann M. Evaluating gambles using dynamics. Chaos 2016;26(2016):023103.
[90] Boillery A, Wald L. Comparison between meteorological re-analyses from ERA-Interimand MERRA and measurements of daily solar irradiation at surface. Renew Energy 2015;75(2015):135–43.
[91] Staffell I, Pfenninger S. Using bias-corrected reanalysis to simulate current and future wind power output. Energy 2016;114(2016):1224–39.
[92] Reichenberg L, Wojciechowski A, Hedenus F, Johnsson F. Geographical aggregation of wind power – an optimization methodology for avoiding low outputs. Wind Energy 2017;20(2017):19–32.

further reading

[93] Norgaard P, Holttinen H. A multi-turbine power curve approach. Proceedings of Nordic Wind Power Conference NWPC'04. 2005. 1.-2.3.2004.
[94] Miao B. Outlook of power generation technology cost in China, Norwegian School of Economics Bergen, Spring 2015; 2015.
[95] Wind-turbine-models.com (2014), Vestas 105-3.3, https://en.wind-turbine-models.com/turbines/891-vestas-v105-3.3, [accessed on November 11th, 2018].